

TOLERANCE

CCR8⁺ decidual regulatory T cells maintain maternal-fetal immune tolerance during early pregnancy

Zhuqing Li^{1,2,3,4,5,6,7,8,†}, Pinxin Si^{1,2,3,4,5,6,7,†}, Tingting Meng^{1,2,3,4,5,6,7,†}, Xiaoran Zhao^{1,2,3,4,5,6,7},
Chendi Zhu^{1,2,3,4,5,6,7}, Dunfang Zhang⁹, Shutong Meng^{1,2,3,4,5,6,7}, Nianyu Li^{1,2,3,4,5,6,7},
Ran Liu^{1,2,3,4,5,6,7}, Tianxiang Ni^{1,2,3,4,5,6,7}, Junhao Yan^{1,2,3,4,5,6,7}, Hongchang Li^{1,2,3,4,5,6,7}, Ning Zhao¹⁰,
Chao Zhong¹¹, Yingying Qin^{1,2,3,4,5,6,7,8}, WanJun Chen^{12*},
Zi-Jiang Chen^{1,2,3,4,5,6,7,13,14*}, Xue Jiao^{1,2,3,4,5,6,7*}

Copyright © 2025 The Authors, some rights reserved; exclusive licensee American Association for the Advancement of Science. No claim to original U.S. Government Works

Regulatory T (T_{reg}) cells play a vital role in maintaining maternal immune tolerance to the semiallogeneic fetus during pregnancy. T_{reg} cell population heterogeneity and tissue-specific functions in the human decidua remain largely unknown. Here, using single-cell transcriptomic and T cell receptor sequencing of human CD4⁺ T cells from first-trimester deciduae and matched peripheral blood of pregnant women, we identified a highly activated, immunosuppressive CCR8⁺ T_{reg} cell subset specifically enriched in the decidua (dT_{reg} cells). CCR8⁺ dT_{reg} cells were decreased in patients with recurrent pregnancy loss (RPL) and an abortion-prone mouse model. Depletion of CCR8⁺ dT_{reg} cells increased susceptibility to fetal loss, with altered decidual immune profiles. Adoptive transfer of CCR8⁺ T_{reg} cells rescued fetal loss in abortion-prone mice. The CCR8 ligand CCL1 was mainly produced by decidual CD49a⁺ natural killer cells and was significantly decreased in patients with RPL. Our data demonstrate that CCR8⁺ dT_{reg} cells are required to maintain maternal-fetal tolerance and highlight potential avenues for RPL therapies.

INTRODUCTION

To achieve a successful pregnancy, a semiallogeneic fetus carrying paternal antigens must be tolerated by the maternal immune system (1). The unique tolerogenic microenvironment in the decidua plays a vital role in recognizing fetal antigens and preventing rejection of the fetus. Disruption of this maternal-fetal immune tolerance is recognized in a variety of reproductive disorders and pregnancy complications, such as recurrent pregnancy loss (RPL), preeclampsia, fetal growth restriction, and preterm birth (2). In particular, RPL, defined

as the loss of two or more pregnancies before 24 weeks of gestation, is a widespread and distressing pregnancy disorder that affects up to 5% of all women attempting to conceive (3). The pathogenesis of RPL is complex and remains undefined for ~50% of patients (4). Although impaired maternal-fetal immune tolerance has been implicated in RPL, the underlying mechanisms remain to be determined.

Forkhead box p3 (Foxp3)-expressing regulatory T (T_{reg}) cells are a nonredundant and immunosuppressive subset of CD4 T cells indispensable for immune self-tolerance and homeostasis (5, 6). During early pregnancy, abundant decidual immune cells (DICs) reside in close contact with infiltrating trophoblasts and actively participate in establishing and maintaining the decidual tolerant microenvironment in early pregnancy. Among these DICs, decidual T_{reg} (dT_{reg}) cells have been suggested to be involved in maintaining maternal immune tolerance and protecting the semiallogeneic fetus in early pregnancy (7). The priming and expansion of T_{reg} cell subsets begin during the menstrual cycle in which conception occurs (8). Upon embryo implantation, maternal T_{reg} cells expand in response to fetal antigens, with dT_{reg} cells comprising 10 to 30% of resident CD4 T cells in the first trimester, and remain enriched throughout pregnancy (8, 9). dT_{reg} cells are positioned to suppress the immune response and inflammation, consequently promoting uterine receptivity to embryo implantation and stimulating vascular remodeling to support placentation in mice (10). Insufficient numbers or impaired functionality of T_{reg} cells in the decidua and peripheral blood has been implicated in individuals with early pregnancy failure or RPL (11–14). T_{reg} cell depletion results in implantation failure and early miscarriage in allogeneic pregnant mice, whereas adoptive transfer of T_{reg} cells can alleviate fetal rejection and pregnancy loss in spontaneous abortion-prone mice (15–17). Therefore, a comprehensive characterization of the regional phenotypic and functional signature of dT_{reg} cells is pivotal to understand decidual adaptation in pregnancy and the pathogenesis of RPL.

¹State Key Laboratory of Reproductive Medicine and Offspring Health, Center for Reproductive Medicine, Institute of Women, Children and Reproductive Health, Second Hospital, Shandong University, Jinan, Shandong 250012, China. ²National Research Center for Assisted Reproductive Technology and Reproductive Genetics, Shandong University, Jinan, Shandong 250012, China. ³Key Laboratory of Reproductive Endocrinology (Shandong University), Ministry of Education, Jinan, Shandong 250012, China. ⁴Shandong Technology Innovation Center for Reproductive Health, Jinan, Shandong 250012, China. ⁵Shandong Provincial Clinical Research Center for Reproductive Health, Jinan, Shandong 250012, China. ⁶Shandong Key Laboratory of Reproductive Research and Birth Defect Prevention, Jinan, Shandong 250012, China. ⁷Research Unit of Gametogenesis and Health of ART-Offspring, Chinese Academy of Medical Sciences (No. 2021RU001), Jinan, Shandong 250012, China. ⁸Department of Reproductive Medicine, Department of Obstetrics and Gynecology, Shandong Provincial Hospital Affiliated to Shandong First Medical University, Jinan, Shandong 250021, China. ⁹Department of Biotherapy, State Key Laboratory of Biotherapy and Cancer Center, Collaborative Innovation Center of Biotherapy, West China Hospital, Sichuan University, Chengdu, Sichuan 610041, China. ¹⁰Analytical Biosciences Limited, Beijing 100191, China. ¹¹Department of Immunology, School of Basic Medical Sciences, NHC Key Laboratory of Medical Immunology, Medicine Innovation Center for Fundamental Research on Major Immunology-Related Diseases, Peking University, Beijing 100191, China. ¹²Mucosal Immunology Section, National Institutes of Dental and Craniofacial Research, National Institutes of Health, Bethesda, MD 20892, USA. ¹³Shanghai Key Laboratory for Assisted Reproduction and Reproductive Genetics, Shanghai, China. ¹⁴Department of Reproductive Medicine, Ren Ji Hospital, Shanghai Jiao Tong University School of Medicine, Shanghai, China.

*Corresponding author. Email: jiaoxue@sdu.edu.cn (X.J.); chenzijiang@hotmail.com (Z.-J.C.); wchen@nih.gov (W.J.C.)

†These authors contributed equally to this work.

Single-cell RNA sequencing (scRNA-seq) has been used to dissect the cellular composition at the maternal-fetal interface in healthy pregnancy and to profile the single-cell landscape of DICs and placental cells' heterogeneity in RPL (18–20). However, because of the scarcity of dT_{reg} cells (<1% of DICs) in the decidua, a comprehensive depiction of dT_{reg} cells remains lacking, limiting the detailed and accurate analyses of bona fide dT_{reg} cells in both normal pregnancy and RPL (8). Therefore, the decidua-specific phenotypes, including the unique transcriptomes and T cell receptor (TCR) repertoires, population heterogeneity, functional adaptation, and tissue-specific factor dependency, that enable them to thrive in deciduae to sustain a healthy pregnancy have not been uncovered.

Here, we provide a comprehensive immune atlas of decidual CD4 T cells by whole transcriptome sequencing with TCR clonotype tracking at a single-cell resolution. We identify a highly stable, activated, and immunosuppressive CCR8⁺ dT_{reg} cell subset. Loss of the CCR8⁺ dT_{reg} cell population was associated with RPL and could increase fetal resorption rate with an altered decidual immune profile, whereas adoptive transfer of CCR8⁺ T_{reg} cells rescued fetal loss in abortion-prone mice. This study expands our fundamental understanding of immune receptivity to embryo implantation and the pathogenesis of RPL and suggests potential strategies for diagnostic and therapeutic development.

RESULTS

Human decidual CD4 T cells are transcriptionally and phenotypically distinct from peripheral blood during early pregnancy

We first aimed to characterize CD4 T cell profiles at the maternal-fetal interface during early pregnancy. We profiled the immune phenotypes and TCR repertoire of CD4 T cells isolated from freshly collected decidua and blood samples of eight women seeking elective pregnancy termination for nonmedical reasons in the first trimester (6 to 8 weeks of gestation) by droplet-based scRNA-seq and TCR V(D)J sequencing (patient characteristics summarized in table S1). CD4⁺CD25^{hi}CD127^{lo} T_{reg} and CD4⁺CD25^{lo/-} conventional T (T_{conv}) cells were sorted by fluorescence-activated cell sorting (FACS) and then pooled at an approximately equal ratio to ensure adequate representation of rare T_{reg} cell subsets (fig. S1A). To further verify the source of samples, we also collected CD45⁺CD14⁻CD4⁻ cells and noted a predominant CD56^{hi}CD16⁻ phenotype specific to decidual natural killer (dNK) cells among the sorted decidual cells, distinct from the canonical CD56^{dim}CD16⁺ blood NK cell [peripheral NK (pNK) cell] phenotype, supporting a decidual origin without blood contamination (fig. S1B) (21).

After filtering for quality control and data integration, we obtained a total of 48,300 high-quality cells from eight donors (fig. S1C). Subsequent dimensional reduction via t-distributed stochastic neighbor embedding (t-SNE) and graph-based Louvain clustering identified 17 distinct clusters of CD4 T cells (Fig. 1A) (22). The cell types comprising each cluster were defined according to their most differentially expressed genes (DEGs) in conjunction with canonical functional markers and annotated on the basis of their specific signature genes (Fig. 1, B and C, and data file S1). The total set of clusters included 11 T_{conv} cell subsets [naïve T cells (T-C01), central memory T cells (T-C02), quiescent T cells (T-C03), effector T cells (T-C04, T-C08), T helper 1 (T_{H1})-like cells (T-C05 to T-C07), cytotoxic T cells [cytotoxic T lymphocytes (CTLs)] (T-C09), NK T

cells (NKTs) (T-C10), and type I T_{reg} (Tr1) (T-C17)] as well as six T_{reg} cell subsets [naïve or resting T_{reg} cells (T-C11 and T-C12) and effector T_{reg} cells (T-C13 to T-C16)].

Most clusters exhibited preferential tissue distribution patterns (Fig. 1D and fig. S1C), implying markedly distinct T cell phenotypes between the decidua and peripheral blood. Naïve T cells (T-C01-TCF7) showed preferential distribution in blood ($R_{O/E}$ values of 1.971), whereas T_{H1}-like clusters (T-C05-BHLHE40, T-C06-KLRB1, and T-C07-XCL2) appeared to be enriched in deciduae, with $R_{O/E}$ values >1. We observed that a T_{H1}, rather than T_{H2} or T_{H17}, expression pattern was predominant among the effector T clusters in deciduae (fig. S1, D and E), suggesting that a T_{H1}-mediated immune response was dominant during the peri-implantation period (23). In addition, a T-C09-TOX cluster was identified with a high expression of markers associated with CD4⁺ CTLs, such as *GZMK* and *GZMB* (fig. S1F). T-C09-TOX CTLs were also enriched for T cell exhaustion markers such as *EOMES* (eomesodermin), *TIGIT* (T cell immunoreceptor with immunoglobulin and immunoreceptor tyrosine-based inhibitory motif domains), *PDCD1* (programmed cell death 1), and *TOX* (thymocyte selection associated high mobility group box) (fig. S1, F to H), suggesting that this subpopulation could tightly suppress the cytotoxic function to preserve immune homeostasis, especially in tolerance toward the fetus (24). Furthermore, a rarely reported CD4⁺ NKT cluster (T-C10-KLRD1) was detected that phenotypically resembled decidual tissue-resident NK (trNK) cells, with a high expression of inhibitory receptors *KLRD1*, *KLRC1*, *KLRK1*, *KIR2DL1*, and *KIR2DL3*, the transcription factor *EOMES*, and cytotoxic effector molecules *GZMB* and *GZMK* (fig. S1, F and I) (25).

We next sought to characterize the TCR repertoire present in decidual CD4⁺ T cells. We obtained 37,440 cells with TCRαβs, including 29,834 cells harboring unique TCRs and 7606 harboring repeated TCRs, indicative of clonal expansion. This likely expansion was observed in CD4⁺ T cells from deciduae and matched blood, with the clonal size ranging from 2 to 127 (fig. S1J). The clonal expansion ability of decidual T (dT) cells, mainly in T_{H1}-like T cells, CTLs, NKTs, Tr1s, and two dT_{reg} cell subsets, was higher than that of most peripheral blood T cell subsets indicated by STARTRAC expansion indices (Fig. 1, E to G, fig. S1K, and data file S2), implying their greater capacity for expansion in response to fetal and placental antigens. These results indicate that CD4⁺ T cells emerge in the decidua during early pregnancy, resulting in a distinct local tissue profile.

dT_{reg} cells have an activated and immunosuppressive phenotype

Considering the critical role of T_{reg} cells in maintaining maternal-fetal immune tolerance, we next characterized the immune profile of decidua-associated T_{reg} cells. As a reference, we also analyzed the T_{conv} cells present in the decidua (dT_{conv} cells) and peripheral blood (bT_{conv} cells). A total of six clusters with a high expression of *IL2RA* and *FOXP3* were defined as T_{reg} cells (T-C11 to T-C16) (Fig. 2A and fig. S2A), among which four clusters (T-C11 to T-C14) were mainly detected in peripheral blood and two (T-C15 and T-C16) were preferentially enriched in the decidua (fig. S2B). More specifically, naïve subsets of T_{reg} cells in peripheral blood (bT_{reg} cells) (T-C11-LEF1 and T-C12-FCRL3) were defined by their expression of naïve marker genes, including *NOSIP*, *SELL*, *LEF1*, *TCF7*, and *CCR7* (26), whereas T-C13-CD52 and T-C14-CCR10 exhibited an increased expression

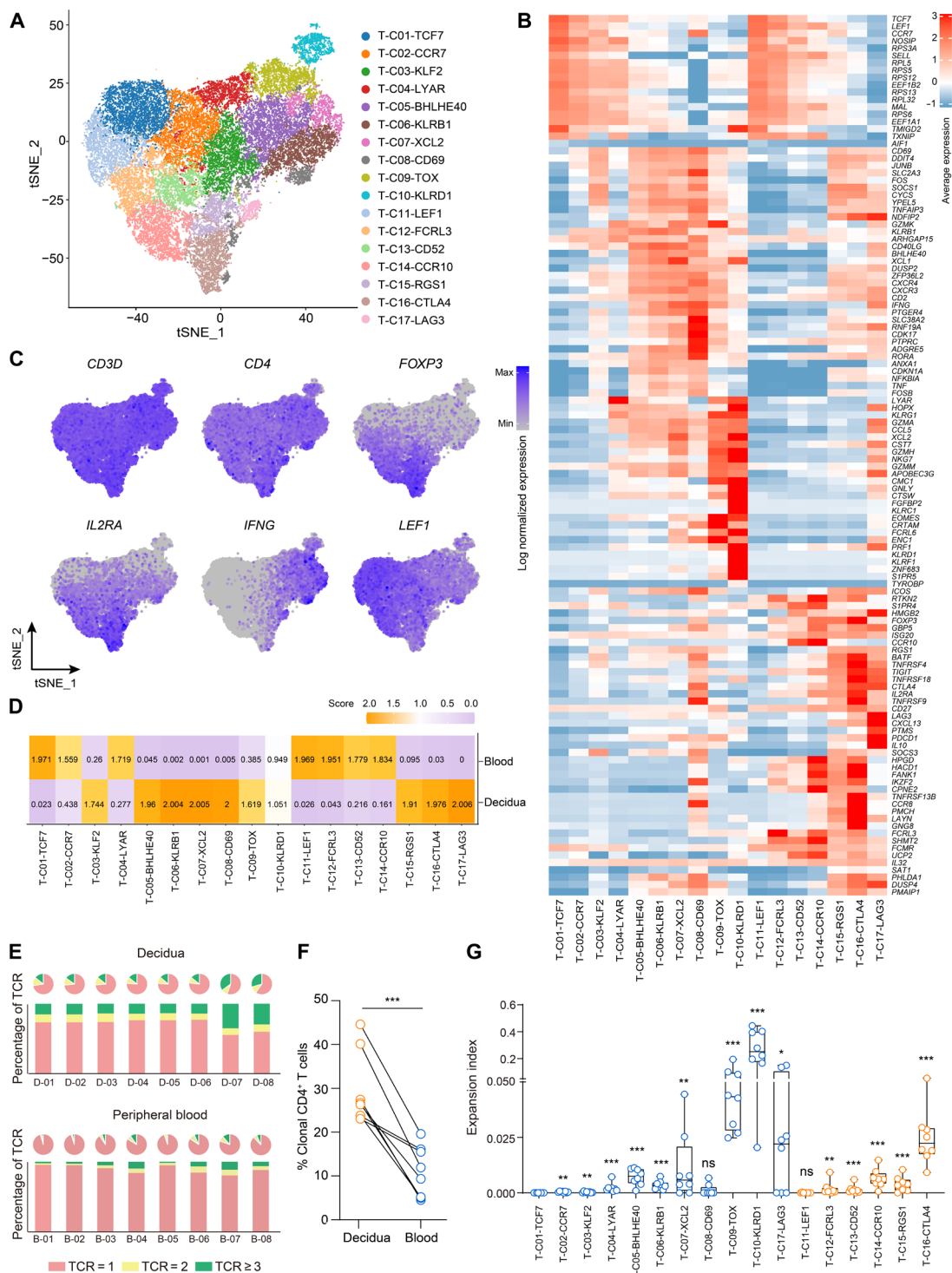


Fig. 1. Human decidua CD4⁺ T cells are transcriptionally and phenotypically distinct from peripheral blood during early pregnancy. (A) t-SNE projection of 48,300 single cells in a total of eight individuals showing the formation of 17 clusters of CD4⁺ T cells, including 6 for T_{reg} cells and 11 for T_{conv} cells. Each dot corresponds to one single cell, colored according to cell cluster. (B) Gene expression heatmap of CD4⁺ T cell clusters. (C) Expression levels of functionally indicative genes illustrated in t-SNE plots. (D) Tissue distribution preference of each cluster shown as a STARTRAC observed/expected distribution score ($R_{O/E}$). $R_{O/E} > 1$ indicates enrichment. (E) TCR distribution of CD4⁺ T cells across different samples. Unique (TCR = 1) and clonal (TCR ≥ 2) TCRs are labeled with different colors. D, decidua; B, blood. (F) Proportion of clonal CD4⁺ T cells in the decidua and matched peripheral blood. (G) Clonal expansion levels of CD4⁺ T cell clusters quantified by STARTRAC expansion indices for each patient. Data shown in (E) to (G): $n = 8$. Data are presented as the means ± SD and were analyzed by paired Student's *t* test (F) or Wilcoxon signed-rank test to assess differences in STARTRAC expansion indices (G). * $P < 0.05$, ** $P < 0.01$, and *** $P < 0.001$. See also fig. S1.

of T_{reg} cell functional markers, such as *TIGIT*, *IL2RA*, *PDCD1*, and human leukocyte antigen class II molecules (27, 28), characteristic of effector T_{reg} cells in peripheral blood (Fig. 2A). In contrast with bT_{reg} cells, the two clusters of dT_{reg} cells (T-C15-RGS1 and T-C16-CTLA4) uniquely exhibited up-regulation of several genes associated with an activated state and immunosuppressive function, such as *CTLA4*, *TIGIT*, *PDCD1*, *ICOS*, *TNFRSF18*, *TNFRSF4*, and *ENTPD1* (29–33). Comparison of transcriptional profiles between dT_{reg} and bT_{reg} cells identified 158 up-regulated DEGs in the dT_{reg} cell cluster [$P < 0.05$ and \log_2 fold change (FC) > 0.5] (Fig. 2B and data file S3). Pathway enrichment analyses of DEGs showed that dT_{reg} cells were enriched in pathways related to negative regulation of the immune system process, consistent with their immunosuppressive function, regulation of lymphocyte cell-cell adhesion, and positive regulation of cytokine production, indicating their specific function in the decidual microenvironment compared with bT_{reg} cells (fig. S2C and data file S4).

To validate the sequencing and the specific features of dT_{reg} cells, we then collected decidua and peripheral blood samples from women with a healthy early pregnancy and investigated the phenotype of dT_{reg} cells using flow cytometry. Consistent with the transcriptomic profiles, several markers of T_{reg} cell stability and suppressive factors were significantly enriched in dT_{reg} compared with bT_{reg} cells, including Foxp3; CD25 (encoded by *IL2RA*); CD39 (encoded by *ENTPD1*), which can promote the accumulation of adenosine and maintain an immunosuppressive microenvironment (33); co-inhibitory receptors PD-1 and TIGIT, which are related to the immunosuppressive function of T_{reg} cells (29, 30); costimulatory factors OX40 (encoded by *TNFRSF4*), GITR (glucocorticoid-induced tumor necrosis factor receptor-related protein, encoded by *TNFRSF18*), and ICOS (inducible T cell costimulator), which participate in the differentiation, proliferation, and activation of T_{reg} cells (34); and the immunosuppressive cytokine interleukin-10 (IL-10) (Fig. 2, C to E, and fig. S2D). Moreover, dT_{reg} cells showed high expression of the proliferation marker Ki-67 and contained a relatively small proportion of CD45RA⁺ naïve cells (Fig. 2F). Furthermore, the proportion of clonal population in dT_{reg} cells was significantly higher than that in bT_{reg} cells, further illustrating the increased activity and proliferation of dT_{reg} cells in response to fetal antigens (Fig. 2G). In addition, we identified several transcription factors that were highly expressed in the dT_{reg} cell population (Fig. 2H), including EOS (encoded by *IKZF4*), which regulates immunomodulatory function in T_{reg} cells (35); BATF (basic leucine zipper activating transcription factor–like transcription factor), which maintains the function of tissue-resident T_{reg} cells (36); and TOX, which participates in CTL exhaustion (37).

To define decidua-specific T_{reg} cell programs, we analyzed DEGs that were uniquely up-regulated in clonal dT_{reg} compared with bT_{reg} and dT_{conv} cells and excluded DEGs up-regulated in bT_{reg} versus bT_{conv} cell comparisons (fig. S2E and data file S5). This analysis revealed nine candidate proteins, including *TNFRSF18*, *TNFRSF9*, *AC133644.2*, *CCR8*, *GEM*, *PMA1P1*, *PHLDA1*, *ACP5*, and *CTSC* (fig. S2F). Among these, the costimulatory molecule *TNFRSF9*, chemokine receptor *CCR8*, and genes with unknown roles in T_{reg} cell biology, including *PHLDA1* and *GEM*, together comprised an apparent decidua-specific T_{reg} cell core transcriptional program.

In addition to these gene expression signatures, we also explored TCR diversity and found that the diversity of dT_{reg} cells was relatively

lower than that of bT_{reg} cells, whereas no difference was observed in either total CD4⁺ T cells or T_{conv} cells between the decidua and peripheral blood (fig. S3A). Principal components analysis (PCA) of the combined V-J frequency profiles showed a significant bias in specific TCR usage in dT_{reg} versus bT_{reg} cells and dT_{conv} but not dT_{conv} versus bT_{conv} cells. In addition, dT_{reg} cells appeared to show a preferential usage bias for V and J genes [odds ratio (OR) > 1] compared with bT_{reg} and dT_{conv} cells (Fig. 2I and fig. S3, B and C), further emphasizing the highly specific function of dT_{reg} cells in fetal antigen recognition and mediating a tolerant immune response at the maternal-fetal interface. These results reveal decidua-specific characteristics of dT_{reg} cells, highlighting their activated phenotype and immunosuppressive potential.

dT_{reg} cells exhibit heterogeneity and distinct developmental trajectories

To investigate the intrinsic heterogeneity and potential functional subtypes of dT_{reg} cells, we next compared transcriptomic profiles and phenotypes between the T-C16-CTLA4 and T-C15-RGS1 dT_{reg} cell populations. DEG analysis uncovered several predominantly up-regulated genes enriched in T-C16-CTLA4 T_{reg} compared with T-C15-RGS1 T_{reg} cells, mainly canonical dT_{reg} cell signature markers including *TIGIT*, *CTLA4*, *CCR8*, *TNFRSF4*, *TNFRSF9*, and *TNFRSF18* (Fig. 3A and data file S6), indicative of a highly suppressive phenotype. In addition, T-C16-CTLA4 T_{reg} cells also showed a higher percentage of clonal T_{reg} cells and STARTRAC expansion indices, as visualized in the ball-packing plot (Figs. 1H and 3B and fig. S4A). These results indicate that T-C16-CTLA4 T_{reg} cells are likely the main functional subset of dT_{reg} cells that respond to fetal antigens during early pregnancy.

We then combined gene expression and TCR data to dissect the differentiation trajectories of dT_{reg} cell subsets. T cells bearing identical TCR $\alpha\beta$ s might be developmentally connected, and we identified a total of 123 TCR $\alpha\beta$ s that were shared between decidua and peripheral T_{reg} cells, with T-C14-CCR10 clusters from different tissues showing the greatest overlap (Fig. 3C and fig. S4B). Analysis of STARTRAC transition scores further implied that the T-C16-CTLA4 cluster was developmentally connected with other individual T_{reg} cell clusters, especially the T-C15-RGS1 cluster (transition score, 0.105; $P < 0.0001$) (Fig. 3D). We then applied RNA velocity analysis embedded on a diffusion map to infer the likely fate of cells (38), which revealed a gradual flow from peripheral naïve T-C11-LEF1 and T-C12-FCRL3 clusters to the effector T-C14-CCR10 cluster and lastly into the decidua T-C16-CTLA4 cluster (Fig. 3E). This finding implied a peripheral origin with a subsequent tissue adaptation process for T-C16-CTLA4 dT_{reg} cells. Alternatively, this combined analysis also uncovered connections between T-C16-CTLA4 dT_{reg} cells and other decidua CD4 clusters, such as T-C03-KLF2-quiescent T_{conv} cells (fig. S4, C and D), suggesting that we cannot exclude the possibility of T-C16-CTLA4 dT_{reg} cells developing from T_{conv} cell populations resident in the decidua. Within the T-C16-CTLA4 dT_{reg} cell subset, we were unable to identify any shared TCRs between the decidua and peripheral blood populations (Fig. 3, C and F), and the T-C16-CTLA4 dT_{reg} cell subset exhibited a high expression of genes associated with tissue residency (*CXCR3*, *CXCR6*, and *ENTPD1*) and a low expression of genes related to T_{reg} cell migration (*S1PR1*, *CCR7*, and *SELL*) (Fig. 3G and fig. S4E), indicating that T-C16-CTLA4 dT_{reg} cells may remain within the decidua as a “tissue-resident” subset.

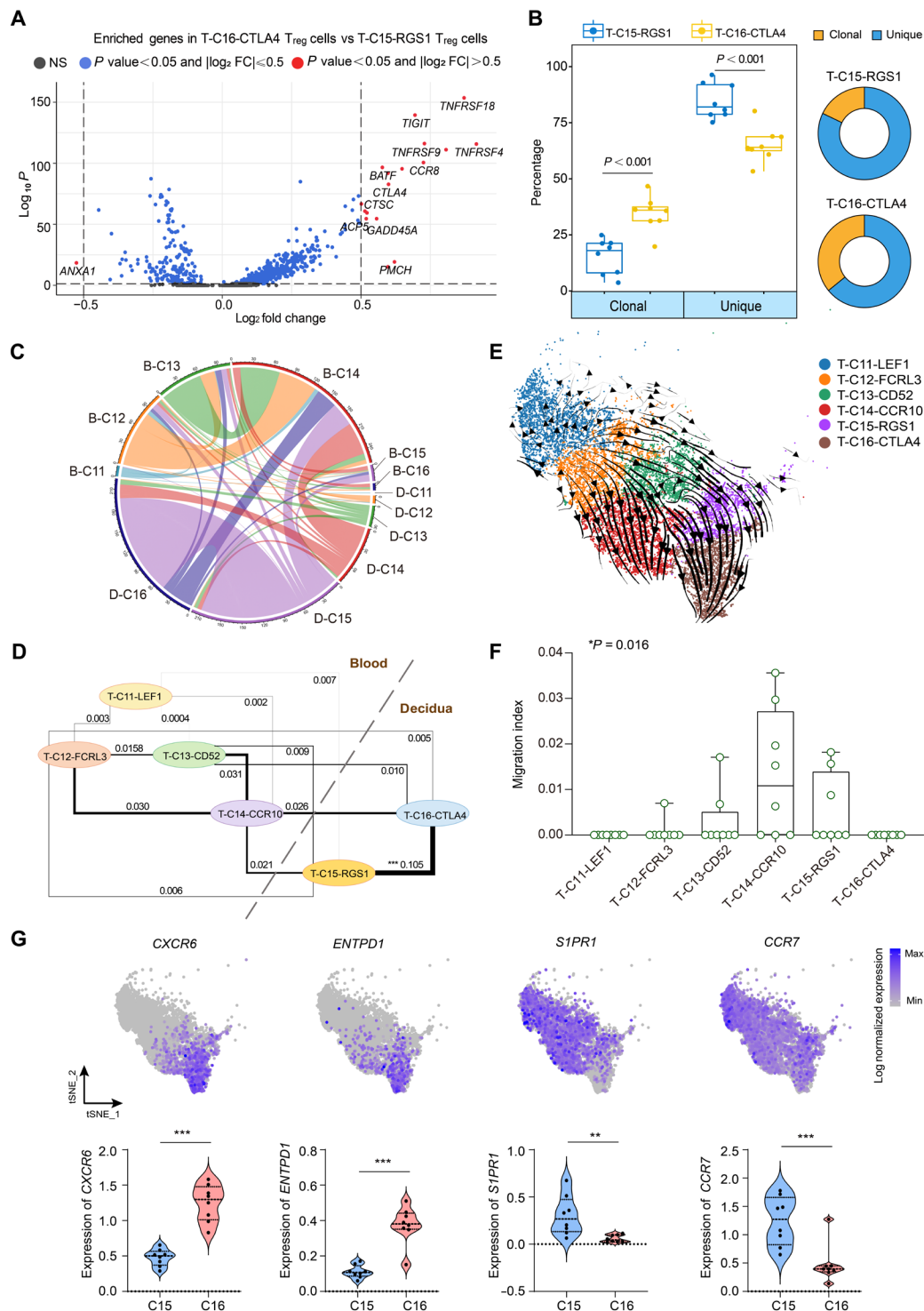


Fig. 3. dT_{reg} cells exhibit heterogeneity and distinct developmental trajectories. (A) Volcano plot showing DEGs between T-C15-RGS1 and T-C16-CTLA4 subsets of dT_{reg} cells. Each red dot denotes an individual gene with an adjusted P value < 0.05 and $|\log_2 FC| > 0.5$. (B) Percentage of clonal and unique T_{reg} cells in T-C15-RGS1 versus T-C16-CTLA4 cluster. (C) Circos plot of TCR clonal sharing between cells in each T_{reg} cell cluster from decidua and peripheral blood. Each line represents one shared clone. (D) State transition of T_{reg} cell clusters inferred by shared TCRs. The dashed line separates the clusters by the tissue origins. The width of solid lines represents STARTRAC transition scores. (E) Inferred developmental trajectory of dT_{reg} cells by RNA velocity. Arrows denote velocity vectors illustrating potential differentiation paths. (F) Cross-tissue migration for all T_{reg} cell clusters quantified by STARTRAC migration scores for each participant. (G) t-SNE plots and comparison of genes associated with tissue residency (*CXCR6* and *ENTPD1*) and T_{reg} cell migration (*S1PR1* and *CCR7*) in the T-C15-RGS1 versus T-C16-CTLA4 cluster. Data shown in (B), (F), and (G): $n = 8$. Data are presented as the means \pm SD and were analyzed by paired Student's t test [(B) and (G)] or Kruskal-Wallis test [(D) and (F)]. $**P < 0.01$ and $***P < 0.001$. See also fig. S4.

CCR8⁺ dT_{reg} cells represent the major functional T_{reg} cell subset in the human decidua during early pregnancy

Next, we sought to identify specific markers that could potentially distinguish between the T-C15-RGS1 and T-C16-CTLA4 dT_{reg} cell subsets. *CCR8* emerged as a top candidate marker that was preferentially expressed on decidual T-C16-CTLA4 T_{reg} cells (Fig. 4A and fig. S2F). Compared with other canonical key T_{reg} cell markers, such as *FOXP3*, *IL2RA*, *TIGIT*, *CTLA4*, *TNFRSF4*, and *TNFRSF18*, *CCR8* showed greater enrichment and exclusive expression in T-C16-CTLA4 T_{reg} rather than other decidual or peripheral T_{reg} cell clusters (Fig. 4B). Further correlation analysis of transcriptomic profiles revealed that *CCR8* levels were positively correlated with genes related to T_{reg} cell function, such as *FOXP3*, *IL2RA*, and *CTLA4* (Fig. 4C), suggesting that *CCR8* could distinguish this predominant T_{reg} cell population in the decidua. To date, the CCR8⁺ T_{reg} cell subset has been reported as principally enriched in a variety of tumors and represents a stable subtype with enhanced immunosuppressive capacity (39–41). We therefore tested whether dT_{reg} cells could be divided into two distinct subgroups by flow cytometry on the basis of C-C motif chemokine receptor 8 (*CCR8*) expression. We found that whereas ~40 to 70% of dT_{reg} cells collected during early pregnancy were positive for *CCR8* expression, only ~10% of bT_{reg} cells, less than 5% of dT_{conv} cells, displayed *CCR8* expression (Fig. 4D, left). No marked expression of *CCR8* was observed on other DIC populations (NK cells, macrophages, CD8⁺ T cells, B cells, dendritic cells, and neutrophils) (fig. S5A). In addition, the *CCR8* levels detected on positive cells, based on mean fluorescence intensity (MFI), were significantly higher in dT_{reg} cells than in other cell types (Fig. 4D, right). Immunofluorescence staining verified that CCR8⁺ cells were preferentially enriched in dT_{reg} cells isolated in the first trimester of pregnancy (fig. S5B), which was consistent with our observations from scRNA-seq analysis.

We next examined the phenotypic features of CCR8⁺ dT_{reg} cells. The DEGs up-regulated in decidual CCR8⁺ dT_{reg} versus CCR8⁻ dT_{reg} cells were enriched in pathways associated with regulation of T_{reg} differentiation, T cell activation, and tolerance induction (Fig. 4E and data file S7). Similarly, CCR8⁺ dT_{reg} cells contained a higher percentage of cells from clonal expansion than their CCR8⁻ counterparts (Fig. 4F). At the protein level, CCR8⁺ dT_{reg} cells had a significantly higher expression of several markers associated with suppressive function, including *Foxp3*, *CD25*, *GARP* (glycoprotein A repetitions predominant), and *IL-10*, as well as immune checkpoint molecules *CD39*, *CTLA4*, *TIGIT*, and *PD-1* (Fig. 4, G and H, and fig. S5C). Costimulatory activation markers (*OX40*, *GITR*, and *ICOS*) and *EOS* were also enhanced in CCR8⁺ dT_{reg} cells (Fig. 4G and fig. S5D). Consistent with their activated immune phenotype, the naïve T cell marker *CD62L* was decreased in the CCR8⁺ dT_{reg} cell population (fig. S5D). In addition, chemokine receptor proteins *CCR4* and *CXCR6* (C-X-C motif chemokine receptor 6), which play a role in T_{reg} cell migration and retention at the maternal-fetal interface, were also detected at high levels (fig. S5E) (42, 43). Last, CCR8⁺ dT_{reg} cells also expressed high levels of the nuclear high-mobility group box protein *TOX* (fig. S5D), which may promote T_{reg} cell activation instead of exhaustion (44). The mRNA and protein phenotypes of these CCR8⁺ dT_{reg} cells, which suggest a high activation status and enhanced immunosuppressive activity, support their role as the major functional subset of dT_{reg} cells at the maternal-fetal interface in early pregnancy.

CCR8⁺ dT_{reg} cells are reduced in the decidua of patients with RPL and abortion-prone pregnant mice

Given the specific phenotypic characteristics of CCR8⁺ dT_{reg} cells, we further investigated whether deficiency for CCR8⁺ dT_{reg} cells could be associated with abnormalities in maternal-fetal immune tolerance, such as in RPL. First, we compared the number and phenotype of T_{reg} cells from the first trimester decidual samples between women with healthy pregnancy and patients with RPL. The patients with RPL showed a mean age of 34 years and had at least two previous unexplained miscarriages with normal embryo karyotypes. No significant difference was observed in the proportion of total dT_{reg} cells (Fig. 5A), although protein levels of *CD25* and *ICOS* were significantly lower in the dT_{reg} cells of patients with RPL compared with those of healthy women (Fig. 5B). This suggests likely functional impairment of dT_{reg} cells in the patients with RPL. However, we found that the subset of CCR8⁺ dT_{reg} cells, and their corresponding *CCR8* expression levels, was significantly reduced in patients with RPL compared with healthy individuals (Fig. 5C). The expression of *CD25*, *TIGIT*, *CTLA4*, *CD39*, *LAG3*, *ICOS*, *GITR*, *EOS*, and *TOX* in CCR8⁺ dT_{reg} cell population was comparable between groups (fig. S6A). The data suggest that a diminished population of CCR8⁺ dT_{reg} cells could be an important factor in the impaired immunosuppressive function of dT_{reg} cells in patients with RPL.

We then asked whether deficiency for CCR8⁺ T_{reg} cells was associated with pregnancy loss in mice. Before examining this subset in an abortion-prone pregnant (AP) model, we first assessed *CCR8* expression in dT_{reg} cells in mice with normal early pregnancy (NP). Flow cytometry analysis indicated that T_{reg} cells comprised ~10% of the total CD4⁺ T cells in mouse decidua at embryonic day 12.5 (E12.5), higher than that in the spleen and peripheral blood (fig. S6B). Consistent with humans, CCR8⁺ T_{reg} cells constituted ~50% of total dT_{reg} cells, and these dT_{reg} cells exhibited marked up-regulation of *CCR8* relative to T_{reg} cells from peripheral blood and spleen, as well as T_{conv} cell counterparts and other immune subsets in the decidua (Fig. 5, D and E, and fig. S6C). CCR8⁺ T_{reg} cells were enriched in the pregnant decidua but not the virgin uteri of nonpregnant mice (Fig. 5, D and E), further supporting the unique role of this subset in pregnancy. As we observed in women with normal pregnancy, the T_{reg} cell-associated proteins involved in suppressive function (*GITR*, *ICOS*, *CTLA4*, and *CD39*) were also highly expressed on CCR8⁺ dT_{reg} cells compared with the CCR8⁻ dT_{reg} and dT_{conv} cell compartments in mice (fig. S6D). These observations indicate that CCR8⁺ dT_{reg} cells represent a major functional subset enriched in the decidua of both humans and mice.

We next used a well-described murine model of immunological spontaneous abortion. In this model, an abnormal maternal immune response led to the rejection of the fetuses and spontaneous abortion in the CBA/J ♀ × DBA/2 ♂ group (AP) but not in the CBA/J ♀ × BALB/c ♂ group (NP) (Fig. 5, F and G). Although total dT_{reg} abundance was similar between the AP and NP mice (fig. S6E), the CCR8⁺ dT_{reg} subset was significantly decreased in AP mice (Fig. 5H), whereas no differences in peripheral blood or spleen CCR8⁺ T_{reg} populations were detected between groups (Fig. 5I). In addition, functional marker expression in CCR8⁺ dT_{reg} cells did not differ between the AP and NP groups (fig. S6F). These results indicate that CCR8⁺ T_{reg} cells are specifically reduced in the decidua of abortion-prone mice, further supporting an association between deficiency in CCR8⁺ T_{reg} cells in the decidua and pregnancy loss in humans and mice.

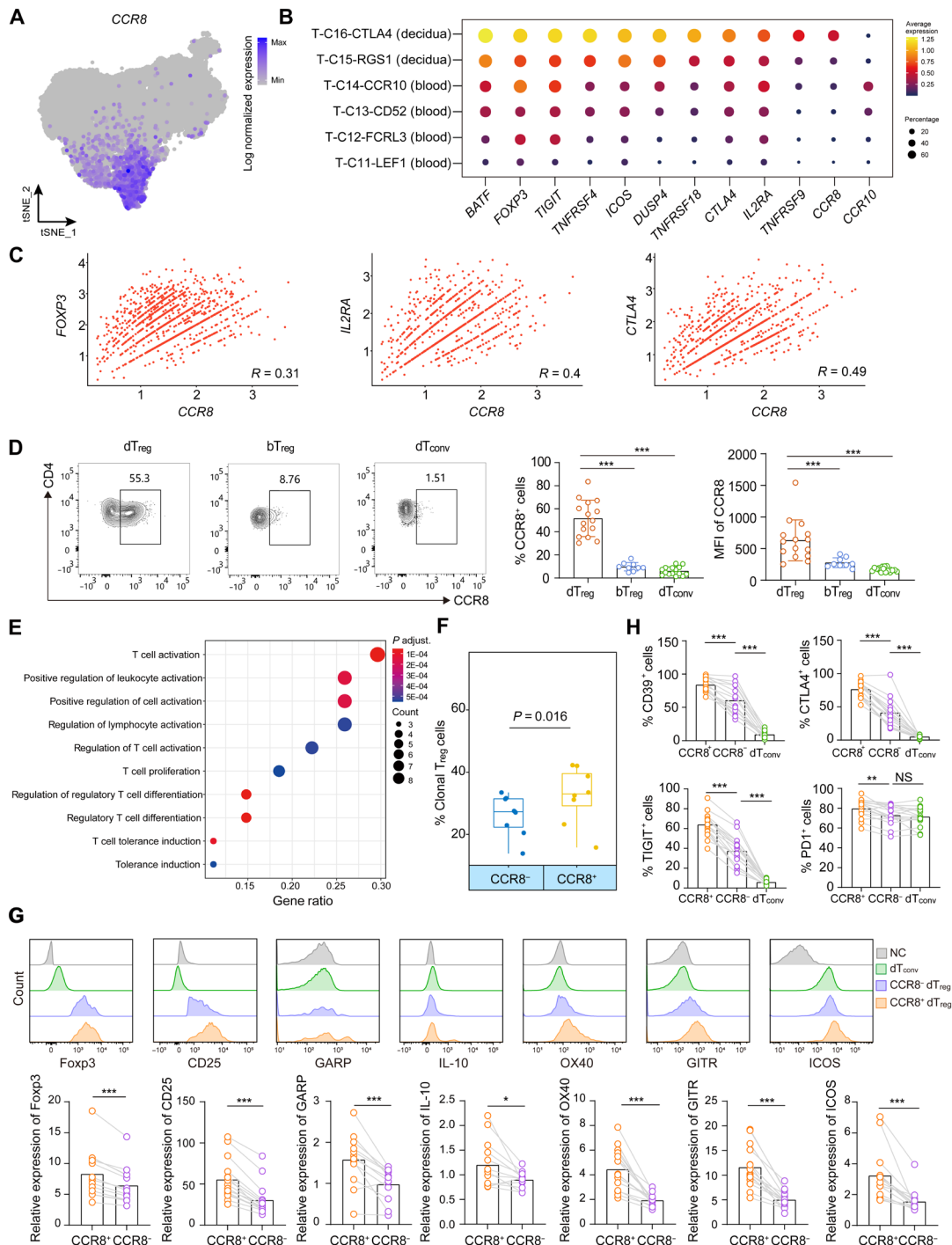


Fig. 4. $CCR8^+$ dT_{reg} cells represent the major functional T_{reg} cell subset in the human decidua during early pregnancy. (A) t-SNE plot showing the expression level of *CCR8*. (B) Dot plot displaying the key T_{reg} cell-related canonical markers in different bT_{reg} and dT_{reg} cell clusters. The dot sizes represent the proportion of cells expressing each gene, and the colors of each dot indicate the average expression levels of each gene. (C) Pearson correlation analysis of the expression levels of *CCR8* and T_{reg} cell signature genes *FOXP3*, *IL2RA*, and *CTLA4*. (D) Representative flow cytometry plots showing the expression of *CCR8* in dT_{reg} , bT_{reg} , and dT_{conv} cells. The percentage of $CCR8^+$ cells and the expression level of *CCR8* were analyzed among dT_{reg} , bT_{reg} , and dT_{conv} cells. MFI was quantified. (E) Most enriched Gene Ontology terms of up-regulated genes in $CCR8^+$ dT_{reg} versus $CCR8^-$ dT_{reg} cells. The dot sizes represent the count of genes expressed in each pathway, and the colors of each dot indicate the adjusted P value. (F) Percentage of clonal cells in $CCR8^+$ dT_{reg} versus $CCR8^-$ dT_{reg} cells ($n = 8$). (G) Flow cytometry analysis of *Foxp3*, *CD25*, *GARP*, *IL-10*, and costimulatory factor expression in $CCR8^+$ dT_{reg} versus $CCR8^-$ dT_{reg} cells. MFI was normalized by dT_{conv} cells. (H) Flow cytometry analysis of the percentage of positive cells for *CD39*, *CTLA4*, *TIGIT*, and *PD-1* in $CCR8^+$ dT_{reg} , $CCR8^-$ dT_{reg} , and dT_{conv} cells. The gray connecting lines in the diagram indicate the matched samples. Data shown in (D), (G), and (H): $n = 16$. Data are presented as the means \pm SD and were analyzed by paired Student's t test [(F) and (G)] or one-way ANOVA using the Bonferroni method for multiple comparisons [(D) and (H)]. * $P < 0.05$, ** $P < 0.01$, and *** $P < 0.001$. See also fig. S5.

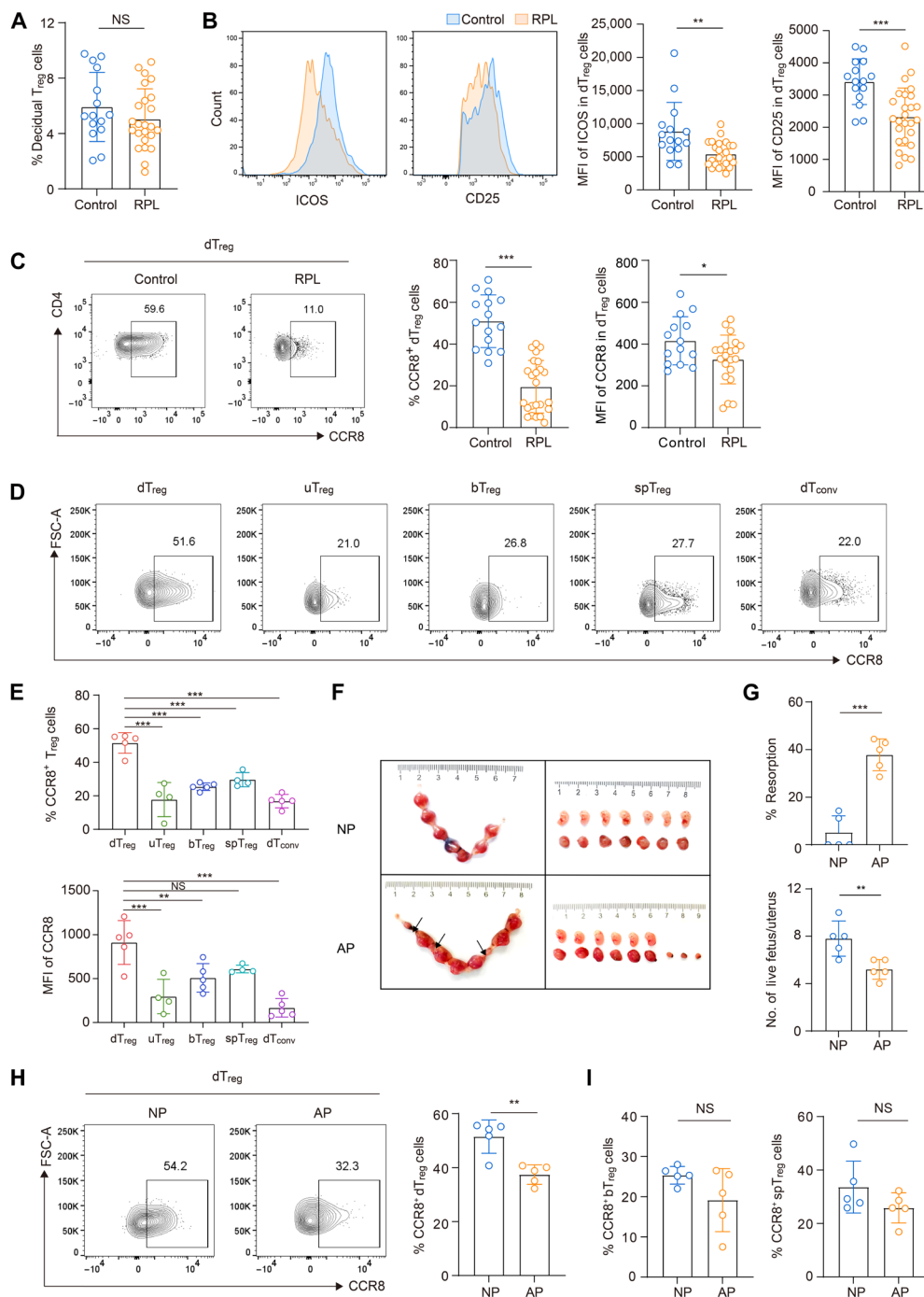


Fig. 5. CCR8⁺ dT_{reg} cells are reduced in the deciduae of patients with RPL and AP mice. (A) Percentage of dT_{reg} cells in patients with RPL and control women. (B) Flow cytometry analysis of ICOS and CD25 expression in dT_{reg} cells from patients with RPL and control women. MFI was quantified. (C) Representative flow cytometry plots showing the expression of CCR8 in dT_{reg} cells from patients with RPL and control women. The percentage of CCR8⁺ dT_{reg} cells and the expression level of CCR8 in dT_{reg} cells were compared between patients with RPL and control women. MFI was quantified. (D) Representative flow cytometry plots of CCR8⁺ cells in dT_{reg}, bT_{reg}, spleen T_{reg} (spT_{reg}), and dT_{conv} cells of normal pregnant mice (♀CBA/J × ♂BALB/c) and uterus T_{reg} (uT_{reg}) cells of nonpregnant (♀CBA/J) mice. (E) Percentage of CCR8⁺ cells and expression level of CCR8 in dT_{reg}, uT_{reg}, bT_{reg}, spT_{reg}, and dT_{conv} cells. MFI was quantified. (F) Establishment of NP (♀CBA/J × ♂BALB/c) and AP (♀CBA/J × ♂DBA/2) mouse models and representative images of implanted embryos in the uterus at E12.5. Black arrows indicate resorbed fetus. (G) Statistical analysis of embryo resorption rate and the number of live fetuses per pregnant mouse in the NP and AP groups. (H) Representative flow cytometry plots showing the expression of CCR8 in dT_{reg} cells from NP and AP mice. The percentage of CCR8⁺ dT_{reg} cells was compared between NP and AP mice. (I) Percentage of CCR8⁺ T_{reg} cells in peripheral blood and spleens from NP and AP mice. Data shown in (A) to (C): control, *n* = 15; RPL, *n* = 26; data shown in (E) to (I): mice each group, *n* = 5. Data are presented as the means ± SD and are representative of three independent experiments, analyzed by Student's *t* test [(A) to (C) and (G) to (I)] or one-way ANOVA using the Bonferroni method for multiple comparisons (E). **P* < 0.05, ***P* < 0.01, and ****P* < 0.001. See also fig. S6.

Depletion of CCR8⁺ dT_{reg} cells leads to pregnancy loss in mice

To further determine whether CCR8⁺ dT_{reg} cell deficiency can increase the risk of maternal-fetal immune intolerance and spontaneous pregnancy loss, we examined the effects of CCR8⁺ dT_{reg} cell depletion on NP in mice. To deplete this population, normal CBA/J female mice with pregnancy from mating with BALB/c males were administered daily intraperitoneal injection of an anti-CCR8 monoclonal antibody (mAb) with antibody-dependent cellular cytotoxicity and blocking activity (45) or a rat IgG2b isotype control from E4.5 to E11.5 (Fig. 6A). Flow cytometry revealed that the proportion of total T_{reg} and CCR8⁺ T_{reg} cells in particular both declined in the deciduae, but not the spleens or peripheral blood, of CCR8 mAb-treated mice (Fig. 6, B to D, and fig. S7A), confirming that this treatment could specifically eliminate CCR8⁺ T_{reg} cells from the decidua microenvironment. The embryo absorption rate increased, whereas the number of live fetuses per uterus decreased by E12.5 in mice lacking the CCR8⁺ dT_{reg} cell subset (Fig. 6, E and F), indicating that deficiency for CCR8⁺ dT_{reg} cells causes pregnancy failure. To further confirm the importance of CCR8⁺ dT_{reg} cells in maintaining pregnancy, we adoptively transferred either CCR8⁺ T_{reg} or CCR8⁻ T_{reg} cells into abortion-prone mice (fig. S7B). We observed that administration of CCR8⁺ T_{reg} cells significantly reduced the resorption rate of the fetus compared with mice treated with phosphate-buffered saline (PBS) or CCR8⁻ T_{reg} cells as controls (fig. S7, C and D). Collectively, these findings suggest that CCR8⁺ T_{reg} cells play a vital role in maintaining maternal-fetal tolerance and preventing abortion.

To determine the mechanisms underlying pregnancy loss stemming from CCR8⁺ dT_{reg} cell deficiency, we next explored changes in the decidua immune microenvironment. We focused on dNK and CD8⁺ T cells, because abnormalities in both subsets have been previously linked to RPL (25, 46). In anti-CCR8 mAb-treated mice, dNK cells expressing cytotoxic molecules were significantly increased compared with isotype-treated controls (Fig. 6, G and H). Granzyme B (GZMB) exerts its cytotoxic effects through caspase cascade activation, Bid protein activation, or DNA fragmentation (47, 48). We observed higher proportions of GZMB⁺CD49a⁻ dNK cells and CD8⁺ dT cells, and GZMB expression was higher in mice treated with anti-CCR8 mAbs (Fig. 6, H and I). No difference was observed in perforin expression between groups (Fig. 6J). Collectively, depletion of CCR8⁺ dT_{reg} cells increased the risk of miscarriage, and this could be through disruption of the maternal-fetal immune tolerance by increased cytotoxic immune cells.

dNK cell-derived CCL1 is decreased in patients with RPL

C-C motif chemokine ligand 1 (CCL1) is the key ligand of CCR8 and plays a critical role in potentiating immune suppressive activity in T_{reg} cells via recruitment and induction of the CCR8⁺ subset and therefore could potentially play a role in the differentiation of CCR8⁺ dT_{reg} cells (49). We first examined CCL1 expression patterns at the maternal-fetal interface in NP by immunofluorescence staining. CCL1 was expressed in deciduae but not villi (Fig. 7A). Further sorting of DICs, decidual stromal cells (DSCs), extravillous trophoblasts (EVTs), and pNK cells revealed that CCL1 was almost exclusively expressed by dNK cells in both humans and mice with normal pregnancy (Fig. 7, B to D), most of which belonged to the regulatory CD49a⁺ subset (Fig. 7, E and F). Previous reports have shown that

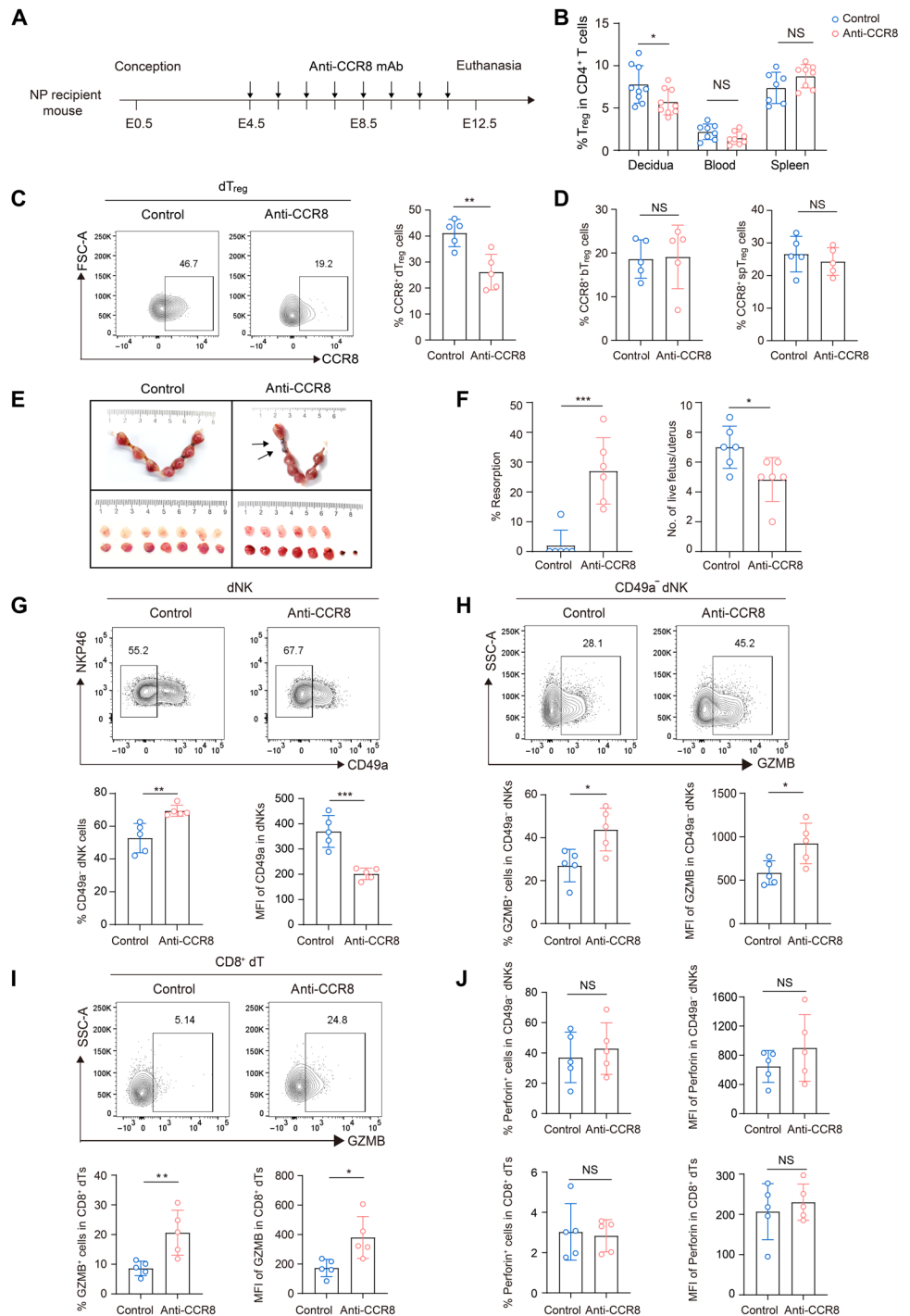
CD49a⁺ trNK cells comprise >90% of human dNK cells but are significantly diminished in patients with RPL (50), suggesting that patients with RPL may be deficient for CCL1 at the maternal-fetal interface. Immunofluorescence staining of first trimester decidua samples collected from five healthy women with early pregnancy and five patients with RPL confirmed that significantly fewer CCL1⁺ cells were present in patients with RPL and that CCL1 expression on dNK cells was significantly reduced compared with decidua from healthy pregnancies (Fig. 7, G and H). These results suggest that CCL1 expression by decidual trNK cells might be necessary for the development of a sufficient CCR8⁺ dT_{reg} cell population to ensure immune tolerance in early pregnancy, whereas inadequate trNK cell-derived CCL1 might result in deficiency for CCR8⁺ dT_{reg} cells, leading to an insufficient immunosuppressive function and potentially contributing to the increased risk of RPL occurrence (fig. S7E).

DISCUSSION

At implantation, embryos express paternally derived alloantigens that can evoke an inflammatory response that potentially threatens reproductive success. dT_{reg} cells are enriched in the decidua during early pregnancy, and in combination with mouse studies of T_{reg} cell depletion and adoptive transfer, the evidence indicates that this subset plays a vital role in maintaining maternal-fetal immune tolerance (8). However, the phenotypic heterogeneity, possible origins, and exact function of these accumulated dT_{reg} cells in early pregnancy remain to be characterized. Here, we performed scRNA-seq to obtain a more comprehensive perspective of decidua-specific T_{reg} cells and identified CCR8⁺ T_{reg} cells as a distinct, highly activated, immunosuppressive subset that is enriched in the decidua during early pregnancy. Diminished CCR8⁺ dT_{reg} cell levels were observed in patients with RPL and abortion-prone mice. Depletion of CCR8⁺ dT_{reg} cells increased susceptibility to fetal loss with altered immune profiles in the decidua microenvironment, and adoptive transfer of CCR8⁺ T_{reg} cells rescued fetal loss in abortion-prone mice. Moreover, deficiency for CD49a⁺ dNK cell-derived CCL1 might contribute to the low abundance of CCR8⁺ dT_{reg} cells detected in patients with RPL. Identification of this previously unidentified CCR8⁺ dT_{reg} cell subset expands our understanding of how immune tolerance is maintained at the maternal-fetal interface during early pregnancy, opening previously unrecognized avenues for RPL diagnosis and therapy.

T_{reg} cell populations are heterogeneous in their phenotype and suppressive function depending on the specific tissue microenvironment in which they reside (51). An increasing number of studies have defined unique, tissue-specific T_{reg} cell subsets in nonlymphoid tissues, including visceral adipose tissue (52), muscle (53), lung (54), skin (55), and the central nervous system (56), where they accumulate to perform important immunoregulatory, tissue homeostatic, and/or regenerative functions (57–59). However, whereas T_{reg} cells in other tissues are becoming increasingly well characterized, a comprehensive picture of decidua-resident T_{reg} cells has remained lacking. Preliminary studies have tried to demonstrate the distinct phenotypes of dT_{reg} cells by limited markers (60, 61), and bulk RNA sequencing data revealed the feature of T_{reg} cells in the peri-implantation endometrium or late gestation decidua, implying that T_{reg} cells can undergo site-specific adaptation during pregnancy (62, 63). Systematic mapping of the cellular landscape of the

Fig. 6. Depletion of CCR8⁺ dT_{reg} cells leads to pregnancy loss in mice. (A) Schematic strategy of anti-CCR8 mAb treatment in normal pregnant (♀CBA/J × ♂BALB/c) mice. (B) Percentage of T_{reg} cells in CD4⁺ T cells from deciduae, peripheral blood, and spleens in pregnant mice treated with anti-CCR8 mAb or isotype controls. (C) Representative flow cytometry plots showing the expression of CCR8 in dT_{reg} cells from mice treated with anti-CCR8 mAb or isotype controls. The percentage of CCR8⁺ dT_{reg} cells was compared between the two groups. (D) Percentage of CCR8⁺ T_{reg} cells in peripheral blood and spleens in mice treated with anti-CCR8 mAb or isotype controls. (E) Representative images of implanted embryos in the uterus at E12.5 from mice treated with anti-CCR8 mAb or isotype controls. (F) Embryo resorption rate and the number of live fetuses per pregnant mouse in pregnant mice treated with anti-CCR8 mAb or isotype controls. (G) Representative flow cytometry plots showing the expression of CD49a in dNK cells (dNKs) from mice treated with anti-CCR8 mAb or isotype controls. The percentage of CD49a⁻ dNK cells and the expression of CD49a in dNK cells were compared between the two groups. (H and I) Representative flow cytometry plots showing the expression of GZMB in CD49a⁻ dNK cells and CD8⁺ dT cells (dT₈) from mice treated with anti-CCR8 mAb or isotype controls. The percentage of GZMB⁺ cells and the expression level of GZMB in CD49a⁻ dNK cells and CD8⁺ dT cells were compared between the two groups. MFI was quantified. (J) Percentage of perforin⁺ cells and expression levels of perforin in CD49a⁻ dNK cells and CD8⁺ dT cells from mice treated with anti-CCR8 mAb or isotype controls. MFI was quantified. Data shown in (B) to (D) and (F) to (J): control, *n* = 9; anti-CCR8, *n* = 9. Data are presented as the means ± SD and are representative of three independent experiments, analyzed by Student's *t* test [(B) to (J)]. **P* < 0.05, ***P* < 0.01, and ****P* < 0.001.



maternal-fetal interface by Vento-Tormo *et al.* (18) identified three dNK subsets that are abnormally distributed in patients with RPL (19, 20). However, the relatively low abundance of dT_{reg} cells (~1% of total immune cells) has thus far precluded in-depth analysis of their features and phenotypic heterogeneity during early pregnancy. Here, by enriching for T_{reg} cells, we could define a core transcriptional program of decidua-specific T_{reg} cells from ~4700 cells, implying substantial heterogeneity and tissue-dependent adaptations

among these cells. Studies have recognized DICs specifically activated for certain preset fetal alloantigens such as ovalbumin (64, 65). We simultaneously performed dNK single-cell TCR profiling and exhibited comprehensive clonal patterns of CD4⁺ dT cells, especially dT_{reg} cells with unique V(D)J usage bias, providing more clues for “fetal-specific” immune responses at the maternal-fetal tolerance. Our subsequent in-depth analysis of phenotypically divergent subsets identified a distinct CCR8⁺ dT_{reg} cell subset with a high

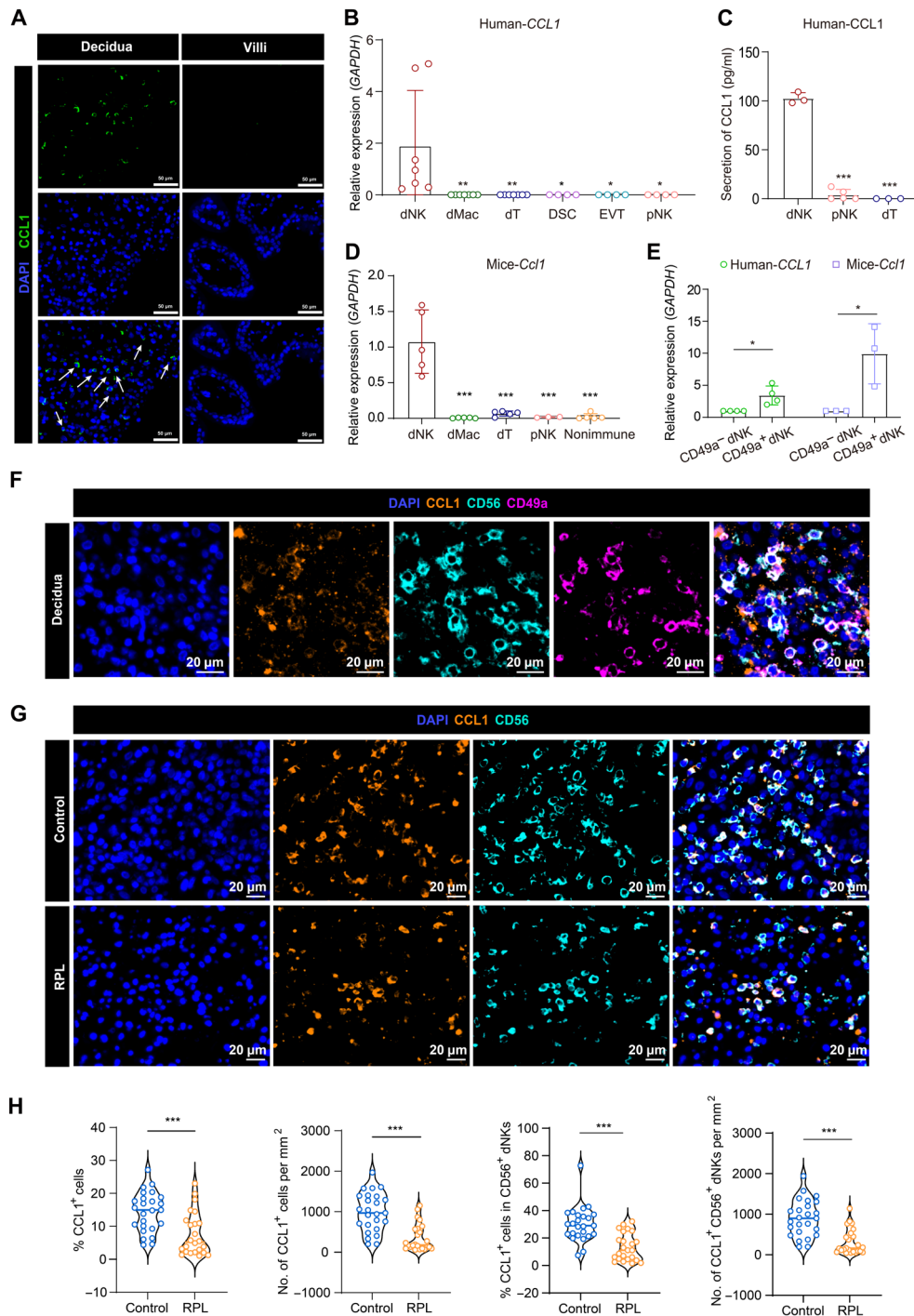


Fig. 7. dNK cell-derived CCL1 is decreased in patients with RPL. (A) Immunofluorescence showing the expression of CCL1 in decidua and villus tissue from women with NP. Scale bar, 50 μ m. (B) qRT-PCR showing the *CCL1* mRNA expression pattern in dNK cells, decidual macrophages (dMacs), dTs, DSCs, EVTs, and pNK cells in women with normal pregnancy. (C) Enzyme-linked immunosorbent assay showing the secretion of CCL1 in dNK cells, pNK cells and dT cells in women with normal pregnancy. (D) qRT-PCR showing the *Ccl1* mRNA expression pattern in dNK cells, dMacs, dT cells, pNK cells, and nonimmune cells in mice with normal pregnancy ($\text{♀C57BL/6J} \times \text{♂C57BL/6J}$) at E12.5. (E) qRT-PCR showing the *CCL1* mRNA expression pattern in CD49a⁺ dNK cells versus CD49a⁻ dNK cells in humans and mice ($\text{♀C57BL/6J} \times \text{♂C57BL/6J}$) at E12.5) with normal pregnancy. (F) Representative immunofluorescence staining of dNK cells from women with NP with CCL1 (red), CD56 (green), CD49a (magenta), and DAPI (blue). Scale bars, 20 μ m. (G and H) Representative immunofluorescence staining and statistical analysis of the quantity of CCL1⁺ cells and CCL1⁺CD56⁺ cells in decidua from five patients with RPL and five control women. Four or five nonoverlapping fields of view randomly selected per sample were applied for statistical analysis. Data shown in (B): $n = 7$; data shown in (C): $n = 5$; data shown in (D): $n = 5$; data shown in (E): human, $n = 4$; mice, $n = 3$; data shown in (H): control, $n = 25$; RPL, $n = 24$. Data are presented as the means \pm SD and were analyzed by one-way ANOVA using the Bonferroni method for multiple comparisons [(B) to (D)] or Student's *t* test [(E) and (H)]. * $P < 0.05$, ** $P < 0.01$, and *** $P < 0.001$.

activation status and enhanced immunosuppressive potential, supporting a possible role as the major functional dT_{reg} cell subset at the maternal-fetal interface in early pregnancy.

The β chemokine receptor CCR8 is a seven-transmembrane protein with four known ligands (CCL1, CCL8, CCL16, and CCL18) and is reportedly expressed specifically by tumor-infiltrating T_{reg} cells (41). CCR8⁺ T_{reg} cells enriched in tumor tissue show a stable phenotype with enhanced immunosuppressive potential compared with CCR8⁻ T_{reg} cells, and a high abundance of tumor-infiltrating CCR8⁺ T_{reg} cells has been significantly associated with poor cancer prognosis (39, 40). Now, it remains unknown whether these cells are present in the decidua and function in pregnancy. To address this gap in knowledge, we comprehensively investigated the phenotypic characteristics of the CCR8⁺ dT_{reg} cell subset and found that this population exhibits enhanced stability, activation, and immunosuppressive potential and represents the major functional subgroup of dT_{reg} cells. Placental and reproductive success require homeostasis of the decidual immune microenvironment at the maternal-fetal interface (66). We found that CCR8⁺ dT_{reg} cell populations are reduced in both patients with RPL and abortion-prone mice, suggesting an association between deficiency for CCR8⁺ dT_{reg} cell subsets and impaired maternal-fetal immune tolerance. However, the decidual tissues were collected after the occurrence of embryo arrest, and it was not clear whether diminished CCR8⁺ dT_{reg} cells are a cause or consequence of miscarriage. Subsequently, anti-CCR8 mAb was applied to selectively deplete CCR8⁺ dT_{reg} cells in normal pregnant mice, resulting in increased fetal resorption and reduced litter size, as well as enhanced cytotoxic phenotypes of NK and CD8⁺ T cells in the decidual microenvironment. Consistently, a recent study reported acquisition of cytotoxic phenotypes in dNK and effector T cells after T_{reg} cell depletion in pregnant mice, indicating a potential association among these cell lineages that might affect pregnancy outcomes (67). Furthermore, adoptive transfer of CCR8⁺ T_{reg} cells significantly rescued fetal loss in abortion-prone mice. These lines of evidence suggest that CCR8⁺ dT_{reg} cells play an essential role in maintaining maternal-fetal immune tolerance, and deficiency for these cells could subsequently lead to pregnancy loss or pregnancy complications.

Targeted therapies that preferentially expand dT_{reg} cells or enhance their suppressive function hold considerable promise as approaches for treating RPL. It is thus vital to clarify the lineage origins and, therefore, molecular programs that drive CCR8⁺ dT_{reg} cell differentiation. On the basis of transcriptomic analysis combined with the TCR repertoire, we speculate that CCR8⁺ dT_{reg} cells might be differentiated from CCR8⁻ dT_{reg} cells, which are largely derived from bT_{reg} cells or, to a limited extent, induced from dT_{conv} cells. This possible scenario supports another recent view that thymus-derived T_{reg} cells are mainly recruited to the uterus in early pregnancy (68, 69). Of note, CCL1, the key ligand of CCR8, has been reported to govern T cell skin homing or tumor recruitment and can also induce CCR8 expression and enhance the immunosuppressive function of T_{reg} cells (70, 71). Therefore, CCL1 could be considered a recruitment and domestication factor for CCR8⁺ dT_{reg} cells. We observed that CCL1 is enriched in deciduae at the maternal-fetal interface and predominantly produced by decidual trNK cells. Furthermore, patients with RPL were previously shown to have decreased decidual trNK abundance, whereas we found that decidual trNK cell-derived CCL1 is also decreased in these patients. These factors together might account for the insufficient immunosuppression arising from CCR8⁺

dT_{reg} cell deficiency that may contribute to the increased risk of RPL occurrence. Further studies are warranted to explore the underlying mechanisms and potential benefits or consequences of CCL1 application as an intervention for RPL.

Although the study provides important insights, there are still some limitations. Given the low abundance of T_{reg} cells infiltrating in deciduae during early pregnancy, we were not able to isolate CCR8⁺ dT_{reg} cells for in vitro experiments to validate their suppressive function. Detailed characterization of CCR8⁺ dT_{reg} cells in patients with RPL remains hindered by inevitable difficulties in obtaining the optimal tissues from RPL cases, because these patients are unlikely to request termination. Consistently, it may not be feasible to predict pregnancy loss on the basis of evaluation of CCR8⁺ T_{reg} cell before pregnancy because of their low proportion detected in menstrual blood. Considering the complexity of fetal antigens, we have not yet been able to illustrate the fetal or placental specificity of dT cells. In addition, further investigation is necessary to define the role and mechanism of CCL1 in pregnancy and in CCR8⁺ dT_{reg} cell induction, in particular. In conclusion, we identified a distinct CCR8⁺ dT_{reg} cell subset crucial for maintaining maternal-fetal tolerance, which further adds to our understanding of the pathogenesis for RPL and provides potential targets for diagnostic or therapeutic applications.

MATERIALS AND METHODS

Study design

The aim was to characterize decidual-specific T_{reg} cell subsets in maintaining maternal-fetal immune tolerance and to propose potential strategies for RPL diagnosis and therapy. With scRNA-seq and single-cell TCR sequencing of CD4⁺ T cells in deciduae and matched blood in women with early pregnancy, we identified a distinct CCR8⁺ dT_{reg} cell population. We then characterized its phenotype and functionality in normal pregnancy and pregnancy failure in both human patients and mouse models. CCR8⁺ T_{reg} cell depletion and adoptive transfer were administered to evaluate the effect and mechanism of CCR8⁺ dT_{reg} cell deficiency on early pregnancy. In addition, we confirmed the source of the CCR8 ligand CCL1 and its deficiency in patients with RPL. Unless noted, all experiments were performed independently at least three times. Investigators were blinded to experimental groups in all experiments involving images and flow cytometry analyses.

Human participants

Participants were recruited from the Center for Reproductive Medicine, Shandong University (SDU) from July 2019 to November 2024. The study was approved by the Institutional Review Board of Center for Reproductive Medicine, SDU (2019IRB73 and 2023IRB91). Written informed consent was provided by each participant. In total, 85 women with a healthy pregnancy (control) and 31 patients with RPL at the first trimester were recruited. RPL was defined as failure of two or more clinically recognized pregnancies with the same partner before 12 weeks. The control group contained normal pregnant women who sought for self-elective pregnancy termination for nonmedical reasons before 12 weeks, and the fetal heartbeat was confirmed by ultrasound before elective termination. Patients with known cause of abortion were excluded, including (i) chromosomal abnormality, (ii) genital malformation, (iii) endometriosis and uterine tumor, (iv) history of autoimmune diseases,

(v) infection in the previous 3 months, and (vi) endocrine disorders (hyperthyroidism and polycystic ovarian syndrome).

Mice

Eight- to 10-week-old DBA/2 (male) and CBA/J mice (female) from Beijing HFK Bioscience (Beijing, China) and 8- to 10-week-old C57BL/6J mice and BALB/c (male) mice from Vital River Laboratory Animal Technology (Beijing, China) were purchased. For mating, virgin CBA/J females were introduced to male BALB/c or DBA/2 mice, and successfully mated mice were confirmed by a visualized copulation plug representing E0.5. In other experiments, female C57BL/6J mice were mated with C57BL/6J males. For all experiments, 9- to 16-week-old female mice were age-matched in different groups, unless otherwise specified. Mice were housed in a controlled environment with specific pathogen-free conditions of 20° to 22°C, 12-hour light/12-hour dark cycle, and 50 to 70% humidity. Food and water were provided ad libitum. All experiments were performed following the animal protocol guidelines of SDU and approved by the Institutional Review Board of Center for Reproductive Medicine, SDU (2019IRB73 and 2023IRB91). Female CBA/J mice were used for dT_{reg} cell characterization, the abortion-prone mouse model, anti-CCR8 mAb treatment, and adoptive transfer experiments. Female C57BL/6J mice were used for cell sorting to detect the expression of *Ccl1* by quantitative reverse transcription polymerase chain reaction (qRT-PCR).

Abortion-prone pregnancy model

To establish NP and AP mouse models, female CBA/J mice were mated with male BALB/c or DBA/2 mice. E0.5 was defined as the day of detection of a vaginal plug. The pregnant mice were euthanized at E12.5. The number of live fetuses and embryo resorption were observed. The embryo resorption rate (*R*) was calculated as $R = R_e/R_c + F$, where *R_e* is the number of resorbed embryos, and *F* is the number of live embryos.

Anti-CCR8 mAb treatment

The pregnant CBA/J females in the NP model (♀CBA/J × ♂BALB/c) were intraperitoneally injected with 15 μg of anti-CCR8 mAb (SA214G2, BioLegend) or isotype control (RTK4530, BioLegend) from E4.5 to E11.5. Mice were euthanized on E12.5 to evaluate the fetal resorption phenotypes, and the decidua, spleen, and peripheral blood were collected for immune cell profiles.

Adoptive transfer experiment

T_{reg} cells were isolated from the spleens of normal pregnant CBA/J females (♀CBA/J × ♂BALB/c) at E12.5 using a CD4⁺CD25⁺ regulatory T isolation kit (Miltenyi Biotec). CCR8⁺ and CCR8⁻ subsets of T_{reg} cells were sorted by FACS, and 4 × 10⁵ cells were resuspended in sterile PBS (200 μl) and injected into abortion-prone females (♀CBA/J × ♂DBA/2) via the tail vein at E4.5, with PBS injection as a negative control. At E12.5, the mice were euthanized and abortion phenotypes were recorded.

Cell isolation

The human peripheral blood, decidua, and villi were freshly collected at the first trimester. Fresh human decidual tissues were washed, cut into small pieces, and dissociated in RPMI 1640 medium (Gibco) containing type IV collagenase (1 mg/ml; Gibco) and deoxyribonuclease I (0.01 mg/ml; Sigma-Aldrich) at 37°C with

constant agitation for 40 min. The suspensions were filtered through a 70-μm sterile strainer (BD Biosciences) using a syringe plunger, washed, and centrifuged on a discontinuous gradient of 20, 40, and 60% Percoll bulk for 30 min at 800g. The DSCs were acquired from the 20 to 40% interface and DICs from the 40 to 60% interface.

Human primary EVT_s were isolated from explants of first-trimester chorionic villi. Fresh human villi were washed, cut into small pieces, explanted in 60-mm petri dishes precoated with 10% Matrigel (Corning), and cultured in Dulbecco's modified Eagle's medium/F-12 (Gibco) supplemented with 10% fetal bovine serum, penicillin (100 U/ml), and streptomycin (100 μg/ml) for 3 to 4 days. EVT_s were outgrown from villous tissue fragments in the following 5 to 7 days, and the adherent EVT_s were digested with 0.25% trypsin for the following experiment.

Fresh human peripheral blood was collected in K₂ EDTA tubes. An equal volume of PBS was mixed with blood and carefully layered over Ficoll Hypaque solution (MP Biomedicals). After centrifugation for 30 min at 2500 rpm (with no break) at room temperature (RT), the mononuclear cell layer was washed three times with PBS for 10 min at 1500 rpm and resuspended in PBS.

Murine decidual samples were minced and digested with type IV collagenase (1 mg/ml) and deoxyribonuclease I (0.01 mg/ml) in RPMI 1640 medium for 40 min at 37°C and then mashed through 70-μm cell strainers to obtain single-cell suspensions. Murine spleen tissues were minced, passed through the 70-μm cell strainers, and underwent red blood cell lysis using ACK lysis buffer (Gibco). Cells isolated were resuspended for subsequent qRT-PCR, cell sorting, or flow cytometry.

Single-cell sequencing library preparation

Human T_{reg} cells (CD45⁺CD4⁺CD25^{hi}CD127^{lo}), T_{conv} cells (CD45⁺CD4⁺CD25⁻), and monocytes/macrophages (CD45⁺CD14⁺) from decidua and matched peripheral blood at the first trimester were sorted on an Aria Cell Sorter (BD Biosciences). Three types of cells were pooled, counted, and loaded onto a 10x Genomics Chromium Controller instrument for single-cell encapsulation with a 5'VDJ kit (10x Genomics) to recover an estimated 5000 cells per library. Reverse transcription was performed using a T100 thermal cycler (Bio-Rad) according to the manufacturer's protocol, followed by the purification of cDNA with silane magnetic beads. Full-length V(D)J segments were enriched via polymerase chain reaction amplification with primers specific to the TCR constant regions. The enriched products were then subjected to enriched library construction. Library quality and concentration were assessed using an Agilent Bioanalyzer 2100. Libraries were run on a HiSeq X or Novaseq for Illumina PE150 sequencing. Because of the unqualified cell viability after FACS, the dT_{conv} cells of P01 and macrophages of P02 were not pooled and examined in the subsequent single-cell sequencing analysis.

Sequence alignment and data analysis

Sequences were aligned to the ensembl human reference transcriptome using the 10x Genomics Cell Ranger pipeline (version 3.1.0). Quality control and transcriptome analysis of single-cell datasets were performed using the R package Seurat (version 3.2.0). Cells were filtered for quality on the basis of the following criteria: mapping to more than 200 unique genes and the fraction of unique mitochondrial transcripts being less than 10%. The TCR library sequences were processed using the Cell Ranger vdj function supplied with mouse

TCR gene annotations and reference sequence files acquired from the International Immunogenetics Information System database (<https://imgt.org/>) and prepared using the `mkvdjref` function.

Unsupervised clustering analysis and identification of signature genes

After quality control, 33,694 genes and 70,763 cells remained and constituted the expression matrix. The expression matrix was first normalized using the Seurat function `LogNormalize`, and then the highly variable features were identified by the Seurat function `FindVariableFeatures` with the “mvp” method. Next, we performed scaling on the previously identified variable features by the Seurat function `ScaleData`, with the percentage of mitochondrial reads regressed. To reduce the dimensionality of the datasets, the `RunPCA` function was conducted with default parameters. Next, the `ElbowPlot` function was used to identify the proper dimensions of each dataset. Last, we picked the top 10 principal components for the downstream clustering analysis. t-SNE dimensionality reduction and graph-based Louvain clustering were performed on the aligned components using the Seurat functions `RunTSNE` and `FindClusters`. A total of 34 clusters emerged at a clustering resolution of 2.0. The Wilcoxon rank sum test was performed to identify the significantly up-regulated genes in each cluster using the Seurat `FindMarkers` function. In the current study, only 17 clusters of T cells were focused on for the following in-depth analysis.

Tissue enrichment analysis

To quantify the enrichment of immune cell types across the decidua and peripheral blood, we compared the observed and expected cell numbers for each cluster in each tissue according to the following formula as previously described (72), $R_{O/E} = (\text{observed/expected})$, where the expected cell numbers of clusters in a given tissue were calculated with the chi-square test. We assumed that one cluster was enriched in a specific tissue if $R_{O/E} > 1$.

Gene set enrichment analysis (GSEA)

DEGs of cell subgroups were recognized by the `FindMarkers` function provided by Seurat. DEGs were defined by adjusted P value < 0.05 and $\log_2\text{FC} > 0.5$ or other criteria indicated in corresponding descriptions. P values were calculated by Student's t test with Bonferroni correction. GSEA was performed by the R package `clusterProfiler` (version 4.2.2). The gene sets we investigated are listed in data file S8.

TCR analysis

The TCR sequencing data were processed using the Cell Ranger `vdj` pipeline with GRCh38 as a reference. In all TCR contigs assembled, we first discarded those with low confidence or that were non-productive. For T cells with two or more α or β chains assembled, the α - β pair showing the highest expression level (unique molecular identifier) was defined as the dominant α - β pair in the T cell. If two or more cells had identical dominant α - β pairs, the dominant α - β pairs were identified as clonal TCRs, and the T cells were identified as clonal T cells. To integrate TCR results with the gene expression data, the TCR-based analysis was performed only for cells that were identified as T cells. For each cluster, the TCR clonotypes occurring in that cluster were counted. To visualize the distribution of counts in each cluster, the R package `APackOfTheClones` (version 0.1.2; <https://github.com/MurrellGroup/APackOfTheClones>) was used to

generate the ball-packing plot. The Shannon index was used to evaluate TCR diversity and was calculated using the diversity function in the R package `vegan` (version 2.6-4). The same clonal type was detected in different clusters, indicating that there was sharing of TCR between clusters. The TCR sharing between different clusters is shown using a chord diagram visualized by the `chordDiagram` function in the `circlize` package (version 0.4.15).

V-J segment usage

The frequency of V-J combinations was calculated to characterize the difference in TCR usage. PCA analysis was performed on the basis of the V-J combination frequency profile, and the significant difference was calculated using permutational multivariate analysis of variance (PERMANOVA). The OR for a given TCR characteristic and T cell lineage was calculated by counting the number of TCRs with (C^+) and without (C^-) that characteristic within the group1 and group2 repertoires. The OR is then given as

$$\text{OR} = \frac{|C^+ \in \text{Group1}| * |C^- \in \text{Group2}|}{|C^- \in \text{Group1}| * |C^+ \in \text{Group2}|}$$

The numerator is the number of group1 TCRs with a given feature multiplied by the number of group2 TCRs without that feature. The denominator is given by the number of group1 cells without that feature multiplied by the number of group2 with that feature. The OR value and P value were calculated from the `fisher.test` function.

STARTRAC analysis

TCR clonal information and cell cluster annotations were used to perform the STARTRAC analysis as previously described (72). Briefly, the degree of clonal expansion, tissue migration, and developmental transition properties of T cell clusters were determined using three STARTRAC indices—STARTRAC-*expa*, STARTRAC-*migr*, and STARTRAC-*tran*, respectively. The detailed pipeline is available on the website (<https://github.com/Japrin/STARTRAC>).

RNA velocity analysis

RNA velocities were predicted using `scVelo` in the Python program. Briefly, spliced/unspliced reads were annotated by `velocity.py` with `CellRanger`, generating BAM files with an accompanying GTF, and then saved in loom files. The loom files were loaded into the `scvelo` python pipeline using the `scv.read` function to generate count matrices for the spliced and unspliced reads. Next, the count matrices were size-normalized to the median of total molecules across cells. The top 2000 highly variable genes were selected out of those that passed a minimum threshold of 20 expressed counts commonly for spliced and unspliced mRNA. The velocities were obtained by modeling the transcriptional dynamics of splicing kinetics. Last, the directional flow was visualized as streamlines in the t-SNE.

Flow cytometry and FACS

The single-cell suspension was stained for dead cells with the Zombie fixable viability kit (BioLegend) and then incubated with Fc blocker human TruStain FcX (BioLegend) or anti-mouse CD16/32 (BioLegend). Cells were incubated with surface antibodies in FACS buffer (PBS containing 2.5% fetal bovine serum) for 15 min at RT in the dark. For intranuclear staining, cells were fixed and permeabilized with fixation/permeabilization buffer solution of `Foxp3/`

transcription factor staining buffer set (eBioscience) at 4°C for 1 hour and then incubated with the antibodies at 4°C for 1 hour. For intracellular staining, cells were fixed and permeabilized with the fixation/permeabilization buffer solution (BD Biosciences) at 4°C for 20 min and incubated with antibodies at 4°C for 30 min. Stained cells were acquired on an LSR Fortessa (BD Biosciences) for analyzing or a FACS Aria II (BD Biosciences) for cell sorting. Data were analyzed with FlowJo software (version 10.7.2, BD Biosciences). The antibodies used are listed in the key resource table.

Immunofluorescence

Decidual tissues were fixed with 10% neutral formalin at RT overnight, dehydrated, embedded in paraffin, and cut into 5- μ m sections. Each primary antibody was paired with an appropriate secondary antibody and TSA (tyramide signal amplification) fluorophore and singly stained in order in the dark. 4',6-Diamidino-2-phenylindole (DAPI) was used to stain the nuclei. The following antibodies were used: anti-CD56 (1:400, CST), anti-CCL1 (1:50 to 100, Invitrogen), anti-CD49a (1:500, CST), and anti-rabbit IgG H&L (HRP) (1:2000, Abcam). Images were acquired using a Nikon Eclipse Ci-L microscope.

qRT-PCR

Total RNA was isolated using RNeasy Plus kits (QIAGEN), and cDNA was then generated with an Evo M-MLV RT for the polymerase chain reaction kit (Accurate Biology). qRT-PCR was performed in triplicate using SYBR Premix Ex Taq kits (Takara Bio) on a Roche LightCycle 480 (Roche). Target gene expression was quantified after normalization to *GAPDH* expression, and the fold change relative to control was calculated by $2^{-\Delta\Delta CT}$. The primers are listed in the key resource table.

Enzyme-linked immunosorbent assay

The concentrations of CCL1 were determined with the human 1-309/CCL1 ELISA Kit (Thermo Fisher Scientific). Briefly, supernatant samples were incubated for 2 to 2.5 hours at RT and washed. After conjugate incubation for 1 to 2 hours, the substrate was applied for 30 min in the dark, and the reaction was terminated with stop solution. The plates were run on the SpectraMax Plus 384 system (Molecular Devices) at 450 nm. The concentration was calculated according to the calibration curve.

Statistical analysis

Statistical analysis was performed with SPSS 26.0 (SPSS Inc.) and GraphPad Prism 9.4.0. Most experiments included at least three independent samples and were repeated at least three times. Data are presented as the means \pm SD and were compared by Student's *t* test, paired Student's *t* test, Wilcoxon signed-rank test, one-way analysis of variance (ANOVA), or Kruskal-Wallis test, where appropriate. Bonferroni correction was used for pairwise comparisons. Pearson correlation analysis was used to explore the relationship between the expression levels of *CCR8* and *T_{reg}* signature genes. $P < 0.05$ was considered statistically significant.

Supplementary Materials

The PDF file includes:

Figs. S1 to S7
Tables S1 and S2

Other Supplementary Material for this manuscript includes the following:

Data files S1 to S9
MDAR Reproducibility Checklist

REFERENCES AND NOTES

1. M. PrabhuDas, E. Bonney, K. Caron, S. Dey, A. Erlebacher, A. Fazleabas, S. Fisher, T. Golos, M. Matzuk, J. M. McCune, G. Mor, L. Schulz, M. Soares, T. Spencer, J. Strominger, S. S. Way, K. Yoshinaga, Immune mechanisms at the maternal-fetal interface: Perspectives and challenges. *Nat. Immunol.* **16**, 328–334 (2015).
2. D. Alecsandru, A. M. Klimczak, J. A. Garcia Velasco, P. Pirtea, J. M. Franasiak, Immunologic causes and thrombophilia in recurrent pregnancy loss. *Fertil. Steril.* **115**, 561–566 (2021).
3. R. Bender Atik, O. B. Christiansen, J. Elson, A. M. Kolte, S. Lewis, S. Middeldorp, S. McHeik, B. Peramo, S. Quenby, H. S. Nielsen, M. L. van der Hoorn, N. Vermeulen, M. Goddijn, ESHRE guideline: Recurrent pregnancy loss: An update in 2022. *Hum. Reprod. Open* **2023**, hoad002 (2023).
4. R. S. Papas, W. H. Kutteh, A new algorithm for the evaluation of recurrent pregnancy loss redefining unexplained miscarriage: Review of current guidelines. *Curr. Opin. Obstet. Gynecol.* **32**, 371–379 (2020).
5. S. Sakaguchi, N. Mikami, J. B. Wing, A. Tanaka, K. Ichiyama, N. Ohkura, Regulatory T cells and human disease. *Annu. Rev. Immunol.* **38**, 541–566 (2020).
6. S. Sakaguchi, T. Yamaguchi, T. Nomura, M. Ono, Regulatory T cells and immune tolerance. *Cell* **133**, 775–787 (2008).
7. P. C. Arck, K. Hecher, Fetomaternal immune cross-talk and its consequences for maternal and offspring's health. *Nat. Med.* **19**, 548–556 (2013).
8. S. A. Robertson, A. S. Care, L. M. Moldenhauer, Regulatory T cells in embryo implantation and the immune response to pregnancy. *J. Clin. Invest.* **128**, 4224–4235 (2018).
9. L. M. Moldenhauer, M. L. Hull, K. L. Foyle, C. D. McCormack, S. A. Robertson, Immune-metabolic interactions and T cell tolerance in pregnancy. *J. Immunol.* **209**, 1426–1436 (2022).
10. S. A. Robertson, L. M. Moldenhauer, E. S. Green, A. S. Care, M. L. Hull, Immune determinants of endometrial receptivity: A biological perspective. *Fertil. Steril.* **117**, 1107–1120 (2022).
11. S. Mei, J. Tan, H. Chen, Y. Chen, J. Zhang, Changes of CD4⁺CD25^{high} regulatory T cells and FOXP3 expression in unexplained recurrent spontaneous abortion patients. *Fertil. Steril.* **94**, 2244–2247 (2010).
12. C. K. Keller, M. Eikmans, M. P. van der Hoorn, L. Lashley, Recurrent miscarriages and the association with regulatory T cells; A systematic review. *J. Reprod. Immunol.* **139**, 103105 (2020).
13. S. Jameel, R. Bhuwalka, M. Begum, R. Bonu, P. Jahan, Circulating levels of cytokines (IL-6, IL-10 and TGF- β) and CD4⁺CD25⁺FOXP3⁺T_{reg} cell population in recurrent pregnancy loss. *Reprod. Biol.* **24**, 100842 (2024).
14. L. M. Moldenhauer, K. L. Foyle, J. J. Wilson, Y. Y. Wong, D. J. Sharkey, E. S. Green, S. C. Barry, M. L. Hull, S. A. Robertson, A disrupted FOXP3 transcriptional signature underpins systemic regulatory T cell insufficiency in early pregnancy failure. *iScience* **27**, 108994 (2024).
15. V. Aluvihare, M. Kallikourdis, A. Betz, Regulatory T cells mediate maternal tolerance to the fetus. *Nat. Immunol.* **5**, 266–271 (2004).
16. A. C. Zenclussen, K. Gerlof, M. L. Zenclussen, A. Sollwedel, A. Z. Bertoja, T. Ritter, K. Kotsch, J. Leber, H. D. Volk, Abnormal T-cell reactivity against paternal antigens in spontaneous abortion: Adoptive transfer of pregnancy-induced CD4⁺CD25⁺T regulatory cells prevents fetal rejection in a murine abortion model. *Am. J. Pathol.* **166**, 811–822 (2005).
17. R. J. Heitmann, R. P. Weitzel, Y. Feng, J. H. Segars, J. F. Tisdale, E. F. Wolff, Maternal T regulatory cell depletion impairs embryo implantation which can be corrected with adoptive T regulatory cell transfer. *Reprod. Sci.* **24**, 1014–1024 (2017).
18. R. Vento-Tormo, M. Efreanova, R. A. Botting, M. Y. Turco, M. Vento-Tormo, K. B. Meyer, J. E. Park, E. Stephenson, K. Polanski, A. Goncalves, L. Gardner, S. Holmqvist, J. Henriksson, A. Zou, A. M. Sharkey, B. Millar, B. Innes, L. Wood, A. Wilbrey-Clark, R. P. Payne, M. A. Ivarsson, S. Lisgo, A. Filby, D. H. Rowitch, J. N. Bulmer, G. J. Wright, M. J. T. Stubbington, M. Haniffa, A. Moffett, S. A. Teichmann, Single-cell reconstruction of the early maternal-fetal interface in humans. *Nature* **563**, 347–353 (2018).
19. C. Guo, P. Cai, L. Jin, Q. Sha, Q. Yu, W. Zhang, C. Jiang, Q. Liu, D. Zong, K. Li, J. Fang, F. Lu, Y. Wang, D. Li, J. Lin, L. Li, Z. Zeng, X. Tong, H. Wei, K. Qu, Single-cell profiling of the human decidual immune microenvironment in patients with recurrent pregnancy loss. *Cell Discov.* **7**, 1 (2021).
20. F. Wang, W. Jia, M. Fan, X. Shao, Z. Li, Y. Liu, Y. Ma, Y. X. Li, R. Li, Q. Tu, Y. L. Wang, Single-cell immune landscape of human recurrent miscarriage. *Genom. Proteom. Bioinform.* **19**, 208–222 (2021).
21. X. Tong, M. Gao, X. Du, F. Lu, L. Wu, H. Wei, B. Fu, Analysis of uterine CD49a⁺ NK cell subsets in menstrual blood reflects endometrial status and association with recurrent spontaneous abortion. *Cell. Mol. Immunol.* **18**, 1838–1840 (2021).

22. T. Stuart, A. Butler, P. Hoffman, C. Hafemeister, E. Papalexis, W. M. Mauck III, Y. Hao, M. Stoeckius, P. Smibert, R. Satija, Comprehensive integration of single-cell data. *Cell* **177**, 1888–1902.e21 (2019).
23. W. Wang, N. Sung, A. Gilman-Sachs, J. Kwak-Kim, T helper (Th) cell profiles in pregnancy and recurrent pregnancy losses: Th1/Th2/Th9/Th17/Th22/Tfh cells. *Front. Immunol.* **11**, 2025 (2020).
24. L. Hardardottir, M. V. Bazzano, L. Glau, L. Gattinoni, A. Köninger, E. Tolosa, M. E. Solano, The new old CD8+ T cells in the immune paradox of pregnancy. *Front. Immunol.* **12**, 765730 (2021).
25. X. Zhang, H. Wei, Role of decidual natural killer cells in human pregnancy and related pregnancy complications. *Front. Immunol.* **12**, 728291 (2021).
26. X. Guo, Y. Zhang, L. Zheng, C. Zheng, J. Song, Q. Zhang, B. Kang, Z. Liu, L. Jin, R. Xing, R. Gao, L. Zhang, M. Dong, X. Hu, X. Ren, D. Kirchhoff, H. G. Roeder, T. Yan, Z. Zhang, Global characterization of T cells in non-small-cell lung cancer by single-cell sequencing. *Nat. Med.* **24**, 978–985 (2018).
27. M. Peiser, A. Becht, R. Wanner, Antibody blocking of MHC II on human activated regulatory T cells abrogates their suppressive potential. *Allergy* **62**, 773–780 (2007).
28. Y. Luo, C. Xu, B. Wang, Q. Niu, X. Su, Y. Bai, S. Zhu, C. Zhao, Y. Sun, J. Wang, M. Liu, X. Sun, G. Song, H. Cui, X. Chen, H. Huang, H. Wang, M. Han, E. Jiang, L. Shi, X. Feng, Single-cell transcriptomic analysis reveals disparate effector differentiation pathways in human T_{reg} compartment. *Nat. Commun.* **12**, 3913 (2021).
29. J. A. Perry, L. Shallberg, J. T. Clark, J. A. Gullicksrud, J. H. Delong, B. B. Douglas, A. P. Hart, Z. Lanzar, K. O’Dea, C. Konradt, J. R. Kuchroo, D. Grubaugh, A. G. Zaretsky, I. E. Brodsky, R. W. Malefyt, D. A. Christian, A. H. Sharpe, C. A. Hunter, PD-1-PD-1 interactions limit effector regulatory T cell populations at homeostasis and during infection. *Nat. Immunol.* **23**, 743–756 (2022).
30. N. Joller, E. Lozano, P. R. Burkett, B. Patel, S. Xiao, C. Zhu, J. Xia, T. G. Tan, E. Sefik, V. Yajnik, A. H. Sharpe, F. J. Quintana, D. Mathis, C. Benoist, D. A. Hafler, V. K. Kuchroo, T_{reg} cells expressing the coinhibitory molecule TIGIT selectively inhibit proinflammatory Th1 and Th17 cell responses. *Immunity* **40**, 569–581 (2014).
31. E. Ayroldi, U. Grohmann, Exemplifying complexity of immune suppression by a “canonical” speech: A glimpse into TNFRSF-activated signaling pathways in T_{reg} cells. *Eur. J. Immunol.* **50**, 944–948 (2020).
32. P. Kumar, P. Bhattacharya, B. S. Prabhakar, A comprehensive review on the role of co-signaling receptors and T_{reg} homeostasis in autoimmunity and tumor immunity. *J. Autoimmun.* **95**, 77–99 (2018).
33. E. Timperi, V. Barnaba, CD39 regulation and functions in T cells. *Int. J. Mol. Sci.* **22**, 8068 (2021).
34. K. Yates, K. Bi, W. N. Haining, H. Cantor, H. J. Kim, Comparative transcriptome analysis reveals distinct genetic modules associated with Helios expression in intratumoral regulatory T cells. *Proc. Natl. Acad. Sci. U.S.A.* **115**, 2162–2167 (2018).
35. A. S. Gokhale, A. Gangaplara, M. Lopez-Occasio, A. M. Thornton, E. M. Shevach, Selective deletion of Eos (Ikzf4) in T-regulatory cells leads to loss of suppressive function and development of systemic autoimmunity. *J. Autoimmun.* **105**, 102300 (2019).
36. M. Delacher, C. D. Imbusch, A. Hotz-Wagenblatt, J. P. Mallm, K. Bauer, M. Simon, D. Riegel, A. F. Rendeiro, S. Bittner, L. Sanderink, A. Pant, L. Schmideleithner, K. L. Brabant, B. Echtenachter, A. Fischer, V. Giunchiglia, P. Hoffmann, M. Edinger, C. Bock, M. Rehli, B. Brors, C. Schmidl, M. Feuerer, Precursors for nonlymphoid-tissue Treg cells reside in secondary lymphoid organs and are programmed by the transcription factor BATF. *Immunity* **52**, 295–312.e11 (2020).
37. O. Khan, J. R. Giles, S. McDonald, S. Manne, S. F. Ngwi, K. P. Patel, M. T. Werner, A. C. Huang, K. A. Alexander, J. E. Wu, J. Attanasio, P. Yan, S. M. George, B. Bengsch, R. P. Staupé, G. Donahue, W. Xu, R. K. Amaravadi, X. Xu, G. C. Karakousis, T. C. Mitchell, L. M. Schuchter, J. Kaye, S. L. Berger, E. J. Wherry, TOX transcriptionally and epigenetically programs CD8⁺ T cell exhaustion. *Nature* **571**, 211–218 (2019).
38. G. La Manno, R. Soldatov, A. Zeisel, E. Braun, H. Hochgerner, V. Petukhov, K. Lidschreiber, M. E. Kastriti, P. Lönnberg, A. Furlan, J. Fan, L. E. Born, Z. Liu, D. van Bruggen, J. Guo, X. He, R. Barker, E. Sundström, G. Castelo-Branco, P. Cramer, I. Adameyko, S. Linnarsson, P. V. Kharchenko, RNA velocity of single cells. *Nature* **560**, 494–498 (2018).
39. G. Plitas, C. Konopacki, K. Wu, P. D. Bos, M. Morrow, E. V. Putintseva, D. M. Chudakov, A. Y. Rudensky, Regulatory T cells exhibit distinct features in human breast cancer. *Immunity* **45**, 1122–1134 (2016).
40. L. Wang, D. L. Simons, X. Lu, T. Y. Tu, S. Solomon, R. Wang, A. Rosario, C. Avalos, D. Schmolze, J. Yim, J. Waisman, P. P. Lee, Connecting blood and intratumoral T_{reg} cell activity in predicting future relapse in breast cancer. *Nat. Immunol.* **20**, 1220–1230 (2019).
41. J. Korbecki, S. Grochans, I. Gutowska, K. Barczak, I. Baranowska-Bosiacka, CC chemokines in a tumor: A review of pro-cancer and anti-cancer properties of receptors CCR5, CCR6, CCR7, CCR8, CCR9, and CCR10 ligands. *Int. J. Mol. Sci.* **21**, 7619 (2020).
42. J. W. Shi, H. L. Yang, D. X. Fan, S. L. Yang, X. M. Qiu, Y. Wang, Z. Z. Lai, S. Y. Ha, L. Y. Ruan, H. H. Shen, W. J. Zhou, M. Q. Li, The role of CXCL chemokine ligand 16 in physiological and pathological pregnancies. *Am. J. Reprod. Immunol.* **83**, e13223 (2020).
43. C. M. Li, L. Hou, H. Zhang, W. Y. Zhang, CCL17 induces trophoblast migration and invasion by regulating matrix metalloproteinase and integrin expression in human first-trimester placenta. *Reprod. Sci.* 10.1177/1933719113519170 (2017).
44. H. Niu, H. Wang, TOX regulates T lymphocytes differentiation and its function in tumor. *Front. Immunol.* **14**, 990419 (2023).
45. Y. Kidani, W. Nogami, Y. Yasumizu, A. Kawashima, A. Tanaka, Y. Sonoda, Y. Tona, K. Nashiki, R. Matsumoto, M. Hagiwara, M. Osaki, K. Dohi, T. Kanazawa, A. Ueyama, M. Yoshikawa, T. Yoshida, M. Matsumoto, K. Hojo, S. Shinonome, H. Yoshida, M. Hirata, M. Haruna, Y. Nakamura, D. Motooka, D. Okuzaki, Y. Sugiyama, M. Kinoshita, T. Okuno, T. Kato, K. Hatano, M. Uemura, R. Imamura, K. Yokoi, A. Tanemura, Y. Shintani, T. Kimura, N. Nonomura, H. Wada, M. Mori, Y. Doki, N. Ohkura, S. Sakaguchi, CCR8-targeted specific depletion of clonally expanded T_{reg} cells in tumor tissues evokes potent tumor immunity with long-lasting memory. *Proc. Natl. Acad. Sci. U.S.A.* **119**, e2114282119 (2022).
46. Z. Wu, M. Wang, G. Liang, P. Jin, P. Wang, Y. Xu, Y. Qian, X. Jiang, J. Qian, M. Dong, Pro-inflammatory signature in decidua of recurrent pregnancy loss regardless of embryonic chromosomal abnormalities. *Front. Immunol.* **12**, 772729 (2021).
47. S. Afonina, S. P. Cullen, S. J. Martin, Cytotoxic and non-cytotoxic roles of the CTL/NK protease granzyme B. *Immunol. Rev.* **235**, 105–116 (2010).
48. M. Walch, F. Dotiwala, S. Mulik, J. Thiery, T. Kirchhausen, C. Clayberger, A. M. Krensky, D. Martinvalet, J. Lieberman, Cytotoxic cells kill intracellular bacteria through granulysin-mediated delivery of granzymes. *Cell* **157**, 1309–1323 (2014).
49. Y. Barsheshet, G. Wildbaum, E. Levy, A. Vitenshtein, C. Akinseye, J. Griggs, S. A. Lira, N. Karin, CCR8⁺FOXP3⁺ T-reg cells as master drivers of immune regulation. *Proc. Natl. Acad. Sci. U.S.A.* **114**, 6086–6091 (2017).
50. B. Fu, Y. Zhou, X. Ni, X. Tong, X. Xu, Z. Dong, R. Sun, Z. Tian, H. Wei, Natural killer cells promote fetal development through the secretion of growth-promoting factors. *Immunity* **47**, 1100–1113.e6 (2017).
51. J. B. Wing, A. Tanaka, S. Sakaguchi, Human FOXP3⁺ regulatory T cell heterogeneity and function in autoimmunity and cancer. *Immunity* **50**, 302–316 (2019).
52. A. Kallies, A. Vasanthakumar, Transcriptional and hormonal control of adipose T_{reg} heterogeneity and function. *Immunol. Rev.* **324**, 42–51 (2024).
53. J. Wu, B. Ren, D. Wang, H. Lin, Regulatory T cells in skeletal muscle repair and regeneration: Recent insights. *Cell Death Dis.* **13**, 680 (2022).
54. N. Arpaia, J. A. Green, B. Molledo, A. Arvey, S. Hemmers, S. Yuan, P. M. Treuting, A. Y. Rudensky, A distinct function of regulatory T cells in tissue protection. *Cell* **162**, 1078–1089 (2015).
55. N. Ali, B. Zirak, R. S. Rodriguez, M. L. Pauli, H. A. Truong, K. Lai, R. Ahn, K. Corbin, M. M. Lowe, T. C. Scharschmidt, K. Taravati, M. R. Tan, R. R. Ricardo-Gonzalez, A. Nosbaum, M. Bertolini, W. Liao, F. O. Nestle, R. Paus, G. Cotsarelis, A. K. Abbas, M. D. Rosenblum, Regulatory T cells in skin facilitate epithelial stem cell differentiation. *Cell* **169**, 1119–1129.e11 (2017).
56. M. Ito, K. Komai, S. Mise-Omata, M. Iizuka-Koga, Y. Noguchi, T. Kondo, R. Sakai, K. Matsuo, T. Nakayama, O. Yoshie, H. Nakatsukasa, S. Chikuma, T. Shichita, A. Yoshimura, Brain regulatory T cells suppress astrogliosis and potentiate neurological recovery. *Nature* **565**, 246–250 (2019).
57. A. R. Muñoz-Rojas, D. Mathis, Tissue regulatory T cells: Regulatory chameleons. *Nat. Rev. Immunol.* **21**, 597–611 (2021).
58. M. Delacher, M. Simon, L. Sanderink, A. Hotz-Wagenblatt, M. Wuttke, K. Schambeck, L. Schmideleithner, S. Bittner, A. Pant, U. Ritter, T. Hehlhans, D. Riegel, V. Schneider, F. K. Groeber-Becker, A. Eigenberger, C. Gebhard, N. Strieder, A. Fischer, M. Rehli, P. Hoffmann, M. Edinger, T. Strowig, J. Huehn, C. Schmidl, J. M. Werner, B. Brors, C. D. Imbusch, M. Feuerer, Single-cell chromatin accessibility landscape identifies tissue repair program in human regulatory T cells. *Immunity* **54**, 702–720.e17 (2021).
59. R. J. Miragaia, T. Gomes, A. Chomka, L. Jardine, A. Riedel, A. N. Hegazy, N. Whibley, A. Tucci, X. Chen, I. Lindeman, G. Emerton, T. Krausgruber, J. Shields, M. Haniffa, F. Powrie, S. A. Teichmann, Single-cell transcriptomics of regulatory T cells reveals trajectories of tissue adaptation. *Immunity* **50**, 493–504.e7 (2019).
60. T. Dimova, O. Nagaeva, A. C. Stenqvist, M. Hedlund, L. Kjellberg, M. Strand, E. Dehlin, L. Mincheva-Nilsson, Maternal Foxp3 expressing CD4⁺CD25⁺ and CD4⁺CD25⁻ regulatory T-cell populations are enriched in human early normal pregnancy decidua: A phenotypic study of paired decidual and peripheral blood samples. *Am. J. Reprod. Immunol.* **66**, 44–56 (2011).
61. M. Salvany-Celades, A. van der Zwan, M. Benner, V. Setrajic-Dragos, G. H. Bougleux, V. Iyer, E. H. Norwitz, J. L. Strominger, T. Tilburg, Three types of functional regulatory T cells control T cell responses at the human maternal-fetal interface. *Cell Rep.* **27**, 2537–2547 (2019).
62. I. Granne, M. Shen, H. Rodriguez-Caro, G. Chadha, E. O’Donnell, J. J. Brosens, S. Quenby, T. Child, J. H. Southcombe, Characterisation of peri-implantation endometrial T_{reg} and identification of an altered phenotype in recurrent pregnancy loss. *Mucosal Immunol.* **15**, 120–129 (2022).
63. J. Wienke, L. Brouwers, L. M. van der Burg, M. Mokry, R. C. Scholman, P. G. Nikkels, B. B. van Rijn, F. van Wijk, Human Tregs at the materno-fetal interface show site-specific adaptation reminiscent of tumor Tregs. *JCI Insight* **5**, e137926 (2020).

64. D. Lissauer, K. Piper, O. Goodyear, M. D. Kilby, P. A. Moss, Fetal-specific CD8⁺ cytotoxic T cell responses develop during normal human pregnancy and exhibit broad functional capacity. *J. Immunol.* **189**, 1072–1080 (2012).
65. J. M. Kinder, L. H. Turner, I. A. Stelzer, H. Miller-Handley, A. Burg, T. Y. Shao, G. Pham, S. S. Way, CD8⁺ T cell functional exhaustion overrides pregnancy-induced fetal antigen alloimmunization. *Cell Rep.* **31**, 107784 (2020).
66. S. E. Ander, M. S. Diamond, C. B. Coyne, Immune responses at the maternal-fetal interface. *Sci. Immunol.* **4**, eaat6114 (2019).
67. S. L. Hosking, L. M. Moldenhauer, H. M. Tran, H. Y. Chan, H. M. Groome, E. A. Lovell, E. S. Green, S. E. O'Hara, C. T. Roberts, K. L. Foyle, S. T. Davidge, S. A. Robertson, A. S. Care, Treg cells promote decidual vascular remodeling and modulate uterine NK cells in pregnant mice. *JCI Insight* **10**, e169836 (2024).
68. L. M. Moldenhauer, J. E. Schjenken, C. M. Hope, E. S. Green, B. Zhang, P. Eldi, J. D. Hayball, S. C. Barry, S. A. Robertson, Thymus-derived regulatory T cells exhibit Foxp3 epigenetic modification and phenotype attenuation after mating in mice. *J. Immunol.* **203**, 647–657 (2019).
69. S. Saito, Reconsideration of the role of regulatory T cells during pregnancy: Differential characteristics of regulatory T cells between the maternal-fetal interface and peripheral sites and between early and late pregnancy. *Med. Princ. Pract.* **31**, 403–414 (2022).
70. M. Wang, Z. Qin, J. Wan, Y. Yan, X. Duan, X. Yao, Z. Jiang, W. Li, Z. Qin, Tumor-derived exosomes drive pre-metastatic niche formation in lung via modulating CCL1⁺ fibroblast and CCR8⁺ Treg cell interactions. *Cancer Immunol. Immunother.* **71**, 2717–2730 (2022).
71. S. Liu, Z. Tao, J. Lou, R. Li, X. Fu, J. Xu, T. Wang, L. Zhang, W. Shang, Y. Mao, F. Wang, CD4⁺CCR8⁺ Tregs in ovarian cancer: a potential effector Tregs for immune regulation. *J. Transl. Med.* **21**, 803 (2023).
72. L. Zhang, X. Yu, L. Zheng, Y. Zhang, Y. Li, Q. Fang, R. Gao, B. Kang, Q. Zhang, J. Y. Huang, H. Konno, X. Guo, Y. Ye, S. Gao, S. Wang, X. Hu, X. Ren, Z. Shen, W. Ouyang, Z. Zhang, Lineage tracking reveals dynamic relationships of T cells in colorectal cancer. *Nature* **564**, 268–272 (2018).

Acknowledgments: We thank all the patients involved in this study. We thank Y. Wei from Shandong Academy of Sciences and T. Yan and L. Cheng from Shandong University for the help in cell sorting. **Funding:** This work was supported by the National Key Research and Development Program of China (2022YFA1103600 to X.J. and C.Z. and 2022YFC2703800 to Y.Q.), the National Natural Science Foundation of China (82371679 and 82171651 to X.J. and 82421004 and 82125014 to Y.Q.), the Distinguished Young Scholars and Taishan Scholars Program for Young Experts of Shandong Province (ZR2022YQ68 and tsqn202211372 to X.J.), the Shandong Provincial Natural Science Foundation (ZR2023QH337 to Z.L.), and the Research Project on Laboratory Construction and Management at Shandong University (sy20243407 to X.J.). W.J.C. is supported by the Intramural Research Program of NIH, NIDCR. **Author contributions:** X.J., Z.-J.C., and W.J.C. conceptualized the study. Z.L., P.S., T.M., N.Z., D.Z., and C.Z. developed the methodologies. Z.L., P.S., T.M., T.N., and N.Z. conducted the formal analysis. Z.L., P.S., T.M., X.Z., C.Z., S.M., N.L., R.L., T.N., and J.Y. carried out the investigation. Z.L., P.S., T.M., T.N., J.Y., and H.L. provided clinical samples. Z.L., P.S., T.M., N.Z., and X.J. performed the data curation. X.J., Z.-J.C., W.J.C., and Y.Q. supervised the study and provided administration for the study. X.J., C.Z., Y.Q., Z.L., and W.J.C. obtained funding for the study. Z.L., P.S., and T.M. wrote the original draft, and all authors contributed to the approval of the final version of this work. **Competing interests:** The authors declare that they have no competing interests. **Data and materials availability:** scRNA-seq data have been deposited in the Gene Expression Omnibus (GEO) database (accession number: GSE252187). All code and scripts necessary to repeat analysis in this manuscript are available upon request. All other data needed to evaluate the conclusions in this study are present in the paper or the Supplementary Materials. Underlying tabulated data for all figures can be found in data file S9.

Submitted 26 January 2024
 Resubmitted 13 December 2024
 Accepted 18 February 2025
 Published 18 April 2025
 10.1126/sciimmunol.ado2463